



University of
Nottingham
UK | CHINA | MALAYSIA

Mechanistic insights into Cu(II) removal from aqueous solution by *Camellia oleifera* shell–reduced graphene oxide

Thesis submitted to the University of Nottingham for the degree of

Master of Research of Environmental Science and Engineering, September 2022.

Shanshan Jiang

20415332

Supervised by

First supervisor: Jun He

Second supervisor: Yong Sun

Signature _____

Date _____ / _____ / _____

Abstract

The Cu(II) pollution in aquatic environment is becoming a severe health challenge due to its non-biodegradable nature. In this study, for the first time, reduced graphene oxide (rGO) was prepared by *Camellia oleifera* shell (COS) extract in a low-cost and environmentally friendly way and successfully applied for the removal of Cu(II) ion from aqueous solutions. An 85.7% removal efficiency was achieved when the initial concentration of Cu(II) was 10 mg/L with a COS-reduced graphene oxide (COS-rGO) dosage of 0.5 g/L, pH of 5.1, and experimental temperature of 20 °C. To propose a mechanism for the removal of Cu(II) using the COS-rGO, characterization tests as well as thermodynamic and kinetics analyses of the COS-rGO adsorption of Cu(II) were systematically performed. The following major inferences were derived from the results of this study: i) The adsorption of Cu(II) using COS-rGO obeyed pseudo-second-order kinetics as a spontaneous endothermic reaction. ii) According to the results of characterization by using Fourier-transform infrared spectroscopy (FT-IR), scanning electron microscopy (SEM), transmission electron microscopy (TEM), and X-ray diffraction (XRD), it was confirmed that the removal of Cu(II) by COS-rGO was a result of chemical adsorption following a rate-controlled process and Langmuir model was applied to this adsorption process. Therefore, it can be expected that the green synthesis of COS-rGO has potential to be a cost-effective adsorbent for removing Cu(II) from water, which has excellent prospects for waste utilization and pollutant reduction.

Keywords: Cu(II), Reduced graphene oxide, *Camellia oleifera* shell, Green synthesis, Adsorption

Acknowledgement

First of all, I would like to give my heartfelt thanks to all the people who have ever helped me in this paper.

My sincere and hearty thanks and appreciations go firstly to my supervisors, Prof. Jun He and Prof Yong Sun, whose suggestions and encouragements have given me much insight into this study. It has been a great privilege and joy to study under their guidance and supervision. Furthermore, it is my honor to benefit from their personality and diligence, which I will treasure my whole life. My gratitude to them knows no bounds.

Sincere gratitude should also go to my parents for their unfailing and friendly love, also, many thanks for their financial support.

I'm grateful to all my friends and classmates who have kindly provided me assistance and encouragement during the whole study process, which picked me out from a lonely research area.

Last but not least, I am really grateful to all those who devote much time to reading this thesis and give me much advice, which will benefit me in my later study. And thanks for myself, to choose the road which I like.

Content

Abstract	1
List of Tables.....	5
List of Figures	6
1. Introduction	7
1.1 Background and significance of this research	7
1.2 Heavy metal ions in the water environments.....	7
1.3 Introduction to graphene materials and <i>Camellia oleifera</i> shell.....	12
1.4 Information of this research.....	17
2. Methodology	21
2.1 Materials and chemical reagents.....	21
2.2 Experimental instruments.....	21
2.3 Preparation of COS extract.....	22
2.4 Preparation of COS extract–reduced graphene oxide (COS-rGO).....	22
2.5 Characterization.....	22
2.6 Pre-experiment of Cu(II) removal	23
2.7 Design Experiment by Response Surface Methodology (RSM) to Prepare COS-rGO.	24
2.8 Condition optimization of Cu(II) removal.....	25
2.9 Adsorbent regeneration and reuse experiments.....	27
3. Results and discussion.....	28
3.1 Removal results using different materials on Cu(II)	28
3.2 Results of Cu(II) removal by different COS-rGO samples according to Box–Behnken (BBD)	29
3.3 Cu(II) removal by COS-rGO under different experimental conditions.....	32
3.4 Characterization.....	34
3.5 Adsorption kinetics.....	39
3.6 Adsorption isotherms.....	41
3.7 Adsorption thermodynamics	42
3.8 Mechanism of Cu(II) removal using COS-rGO	43
3.9 Recyclability and stability studies	44
4. Conclusions and prospects	46

4.1 Conclusions	46
4.2 Prospects.....	47
Bibliography.....	48

List of Tables

Table 1 Materials and chemical reagents used in this experiment.	21
Table 2 Instruments used in this experiment.	21
Table 3 Variables and their levels in Box–Behnken (BBD) of the experimental conditions for preparing COS-rGO.	25
Table 4 Box–Behnken (BBD) matrix of experimental conditions for preparing COS-rGO.	25
Table 5 Adsorption results of Cu(II) by COS-rGO based on BBD.....	29
Table 6 Analysis of variance (ANOVA) of quadratic model.....	30
Table 7 Kinetics parameters for Cu(II) removal by COS-rGO.	40
Table 8 Isotherm parameters for Cu(II) removal by COS-rGO.....	42
Table 9 Thermodynamic parameters for Cu(II) adsorption using COS-rGO.	43

List of Figures

Figure 1 Adsorption of Cu(II) using different materials.	28
Figure 2 Experimental vs. predicted Cu(II) adsorption values.	31
Figure 3 Surface plots illustrating Cu(II) adsorption influenced by operational factors.	32
Figure 4 Efficiencies of Cu(II) removal by camellia oleifera shell–reduced graphene oxide (COS-rGO) under different conditions.	34
Figure 5 X-ray diffraction (XRD) patterns of graphene oxide and COS-rGO prepared with <i>Camellia oleifera</i> shell (COS).	35
Figure 6 Scanning electron microscopy (SEM) images of (a) graphene oxide (GO) and (b) COS-rGO.	36
Figure 7 Transmission electron microscopy (TEM) images of COS-rGO (a) before and (b) after exposure of Cu(II).	36
Figure 8 Fourier-transform infrared spectroscopy (FT-IR) spectra of COS, GO, and COS-rGO.	37
Figure 9 Raman spectra of GO and COS-rGO.	38
Figure 10 (a) X-ray photoelectron spectroscopy (XPS) survey spectra of COS-rGO before and after exposure to Cu(II). (b) Cu 2p spectrum of COS-rGO after adsorption of Cu(II). C 1s spectrum of COS-rGO (c) before and (d) after adsorption of Cu(II).	39
Figure 11 Proposed mechanisms of Cu(II) removal by COS-rGO.	44
Figure 12 COS-rGO recycling experiment.	45

1. Introduction

1.1 Background and significance of this research

Water pollution has been a severe problem to the environment, human beings, and other organisms for many years. Among all the contaminants in aqueous environments, the presence of heavy metals, including Cu, Cr, Pb, and Ni, is mostly originates from industrialization and agriculture activities, including storage batteries, automobile fuels, coating materials, and the aeronautics and steel industries. These contaminants deserve great attention and need to be removed from polluted environments because of their non-biodegradability and tendency to accumulate in living organisms, even with trace concentrations. The existence of these metallic pollutants has caused great harm to the water ecological balance and may eventually affect human health. It deserves great attention and efficient removal methods due to its difficulty to biodegrade and tendency to accumulate in organisms, even with trace amounts (Chen et al., 2014; Peng et al., 2014). Thus, numerous studies have been devoted to remove toxic metals from water environments. Among the variety of functional materials used in environmental remediation, nanomaterials such as graphene and nano-iron are emerging due to their excellent characteristics, including large specific surface areas, high reactivities, biocompatibility, and adsorption capacities.

1.2 Heavy metal ions in the water environments

1.2.1 Present situation

Rapidly growing industrialization has caused fast economic development, while industrial wastewater containing high concentrations of heavy metals has been wantonly discharged into the natural environment without proper treatment. It is almost not possible for these heavy metals to be naturally degrade, resulting in a gradual increase in their concentrations in the recipient water body, which then significantly affects the balance of the water ecosystem. In addition, these heavy metals will gradually accumulate through the food chain and eventually pose a threat on the health of human beings (Chakravarty et al., 2010).

1.2.2 Sources of copper pollution in water environments

Copper pollution in aquatic systems originates from both natural and anthropogenic sources, mainly including volcanic activities, mining processes, and pesticide use. Copper ions can be present in particularly high concentrations in wastewater discharged from metal processing and electroplating plants, reaching as high as hundreds of milligrams per liter of wastewater.

1.2.3 Significance of heavy metal remediation in water environments

The copper ion is an essential nutrient for human beings for the maintenance of red blood cells, nerve cells, and the immune system when at a proper concentration, but it can become a drinking-water contaminant when its concentration exceeds 2 mg/L based on the standard set by the World Health Organization (Malhotra et al., 2020; WHO, 2017). Copper has been regulated as an aesthetic contaminant with metallic taste by the United States Environmental Protection Agency (USEPA) according to the National Secondary Drinking Water Regulations (NSDWRs) which set the Secondary Maximum Contaminant Level (SMCL) at 1.0 mg/L (US EPA, 2015). If copper-containing wastewater is used for farming and irrigation purposes on agricultural land, it will gradually accumulate in soil and crops, resulting in the poor growth of crops and finally becoming concentrated in the human body. Excessive copper exposure from the human diet will lead to itching, dermatitis, vomiting, cramps, convulsions, and even death. For industrial fields, the concentration of industrial wastewater sometimes reaches 1000 mg/L (GB 25467, 2010; Sun et al., 2021). Thus, to safeguard ecological stability and public safety, copper removal is absolutely imperative and requires further in-depth studies.

1.2.4 Methods of removing heavy metal ions

To date, various studies have been conducted in the wastewater treatment field, especially on the removal of heavy metals through methods including chemical precipitation (Yan et al., 2010), membrane filtration (Gao et al., 2014), ion exchange (Naushad, 2014), and adsorption (Ioannou-Ttota et al., 2019). These methods have been demonstrated to be effective for removing heavy metals.

1.2.4.1 Ion exchange

Ion exchange can reduce heavy metal ions in water by ion exchange between an ion exchange resin and heavy metal ions (Riveros, 2010). This method dates back hundreds of years, when ion exchange was a technique applied for softening water. There have been considerable varieties of ion-exchange materials, including natural and synthetic, organic and inorganic, cationic, and amphoteric materials (Kumar and Jain, 2013). The application of synthetic organic resins, and inorganic three-dimensional matrices materials has been verified for common use as ion-exchange materials with the development of technology (Bashir et al., 2019). The advantages of the ion exchange method are that it bears a remarkable removal effect, high exchange rate, and strong regeneration ability. However, zeolites or organic resins suffer from disadvantages such as low selectivity for heavy metals, and organic–inorganic hybrid materials suffer from long reaction times, long cycles, and complex regeneration processes. It is easy for this method to produce excessive regeneration of waste liquid, causing secondary pollution to the environment. Thus, it is of high significance to find ion-exchange materials with outstanding efficiencies and low costs.

Alyüz and Veli (2009) studied the Dowex HCR S/S cation exchange resin for removing Ni and Zn from wastewater. The results showed a 98% removal efficiency. Lu et al., (2016) used thermal-treated zeolites to remove Pb(II) and Cu(II) and obtained maximum removal capacities at 135.5 and 115.5 mg/g, respectively.

1.2.4.2 Chemical precipitation

Chemical precipitation is a relatively mainstream wastewater treatment method at present. Chemical reagents such as hydroxide and iron salt are used as precipitants for heavy metal ions. These chemical precipitants can form insoluble substances, which can be separated from the aqueous solution by precipitation or filtration to remove heavy metal ions (Schouwenaars et al., 2017). Chemical precipitation is a conventional wastewater treatment method mostly used in industry, involving the adjustment of the pH values to convert heavy metal ions to hydroxide, sulfide, or carbonates, which are then removed by physical methods like sedimentation, flotation, or filtration (Chen et al., 2009; Demopoulos, 2009; Mokone et al., 2010). The advantages of the

chemical precipitation method are that it is simple to perform and that it has a good removal effect and wide pH application range. However, it still has some disadvantages, such as forming secondary pollution, requiring a large equipment area, and having a high treatment cost.

From the study of Chen et al., (2018), Ca(OH)_2 , Na_2CO_3 , and Na_2S were used as the chemical reagents to remove Zn(II) , Cu(II) , and Pb(II) from aqueous solutions via a chemical precipitation method. The removal efficiency reached 99.99% using the three precipitants for Cu(II) and Zn(II) at initial concentrations of 100 mg/L. Zhang and Duan, (2020) studied the preparation of magnesium hydroxy carbonate from low-grade magnesite and its application as a precipitating agent for removing Cr(II) and Fe(II) from wastewater. The removal efficiencies were above 99.9% within 20 min.

1.2.4.3 Membrane filtration

The principle of membrane separation is to use membrane materials with selective permeability to selectively permeate pollutants in water and achieve the removal of pollutants (Hylling et al., 2019). Membrane filtration has good prospects in the field of water pollution remediation owing to the high removal efficiency, low cost, and convenient operation. The disadvantages of this method are limited permeabilities and reusability of membrane materials, though it can be restored by chemicals such as alkali solutions, which will lead to high costs and secondary pollution. Thus, membrane filtration is still far from being a proper method for widespread use.

Almasian et al., (2018) studied the separation performances of Pb(II) and Cd(II) from aqueous solutions using a core-shell nanofibrous membrane made using polyacrylonitrile (PAN)/polyaniline (PANI)-nylon through a coaxial electrospinning method, and used diethylenetriamine (DETA) to modify the surface to increase the hydrophilicity of the membrane. The removal efficiencies reached 89.1%, 96.8%, and 95.1% for bovine serum albumin (BSA), Pb(II) and Cd(II) , respectively. The membrane showed good regeneration properties after alkali treatment, where 87.6% and 86% removal efficiencies for Pb(II) and Cd(II) were reached after 10 filtration cycles.

1.2.4.4 Adsorption

Adsorption is a process that uses an adsorbent to transfer pollutants in water from the liquid phase to the solid phase surface and combine pollutants with an adsorbent through physical or chemical action. Adsorption is now considered to be the most suitable and environmentally friendly method to remove heavy metal ions owing to its easy operation and low cost, and more importantly, the feasibility of recycling used adsorbents as well as recovering heavy metals, which make it an environmentally friendly, economic, and efficient water pollution treatment method (Lata et al., 2015; Oh et al., 2019; Chakravarty et al., 2010; Li et al., 2018). Adsorbents generally have advantages such as large specific surface areas, high adsorption capacities, and high surface activities. The type of adsorbents, the dosage of adsorbent, the composition and concentration of wastewater all have a certain impact on the treatment effect of wastewater containing heavy metals. Currently, the main target is to explore more technologically and commercially feasible and recyclable materials, and the mostly used adsorbents including inorganic adsorbents, organic adsorbents and bio-sorbents (Bilal et al., 2021).

i) Inorganic adsorbents: the inorganic adsorbents used in wastewater treatment mainly include: hydroxyapatite (Nayak and Bhushan, 2021), titanate nano materials (Li et al., 2021), activated alumina (Hao et al., 2009), zeolite (Javed et al., 2015), magnetic graphene oxide composite materials (Gabris et al., 2018), diatomite (Sprynskyy et al., 2015). Kayalvizhi et al., (2022) prepared a biomaterial using activated Sawdust-Chitosan nanocomposite beads (SDNCB) powder to study the adsorption efficiency of Ni (II) and Cu (II). The study showed an excellent removal effect of Ni (II) and Cu (II) which finally was proved to be the strong involvement between the ions and chitosan's functional groups and cellulose.

ii) Organic adsorbents: the organic adsorbents used in wastewater treatment mainly include: lignocellulose (Kayranli et al., 2021), adsorption resin (Aboul-Magd et al., 2016), biochar (Luo et al., 2022). Ye et al., (2021) made the modified montmorillonite with a two-dimensional network structure by modifying the montmorillonite (MMT) and then using the addition of chitosan (CS) to improve the modified material to a three-dimensional network structure with high specific surface areas. This material has been proved to be a better adsorbent in removing Cu (II) ions.

iii) Bio-sorbents: the bio-sorbents used in wastewater treatment mainly include: algae(Farhan et al., 2021), fungi(Anwer and Bushra, 2015), bacteria(Huiping et al., 2013). Meringer et al., (2021) acquired a non-viable *Pseudomonas putida* from agar beads and used it as a bio-sorbent to remove Cu (II) from solution which showed a 60% removal efficiency and a great recyclability with ten absorption/desorption cycles.

1.3 Introduction to graphene materials and *Camellia oleifera* shell

1.3.1 Properties of graphene and its application in environment

In 2004, graphene, with its hexagonal lattice structure of carbon atoms arranged in sp^2 hybrid orbitals, was discovered as a carbon-based nanomaterial with two-dimensional properties by Konstantin Novoselov and Andre Geim (2004) from the University of Manchester through a micro-mechanical stripping method. Graphene has attracted tremendous attention due to excellent characteristics, such as its good thermal conductivity, electrical conductivity, optical properties, and stability, allowing it to exhibit ideal performances in thermal, electrical, mechanical, and optical applications (Novoselov et al., 2004; Velusamy et al., 2021). Many studies have shown that graphene, with a large specific surface, stable chemical properties, and high negative charge density, has a great capacity to coordinate with heavy metal ions and thus, is considered to be a promising adsorbent for removing heavy metal pollutants (Hu et al., 2013; Yang et al., 2012).

Zare Pirhaji et al., (2020) made a nanocomposite material by using graphene quantum dots (GQDs) immobilized onto $NiFe_2O_4$ -halloysite nanotube ($NiFe_2O_4$ -HNT) surfaces and studied the adsorption efficiency of Pb(II) ions. Results showed a 97.14% removal rate of Pb(II) at the maximum adsorption capacity, and the process was mainly bottomed on the complexation interactions between Pb(II) and functional groups on this composite.

1.3.2 Properties of *Camellia oleifera* (*C. oleifera*) shell and its application in the environment

C. oleifera, belonging to the Camellia family, is widely planted in south China with a long cultivation history (Zhang et al., 2011; Zhu et al., 2013). The oil from its seed, which is called tea oil or “Eastern olive oil”, is valuable resource as a high-grade edible oil that contains unsaturated fatty acids, including oleic acid and linoleic acid, which, to some extent, make it much healthier than other edible oils (Ong et al., 2017; Sahari et al., 2004; Zhang et al., 2006). The *C. oleifera* seed shell represents nearly 60% of the whole fruit weight, containing abundant chemicals such as phenols, terpenes, flavonoids, and polysaccharides. Most seed shells are directly discarded or burned, causing both environmental pollution and a large waste of resources (Liu et al., 2019a; Sramala et al., 2016). In the past, the shells were usually burned for warmth in rural villages. Today, electricity is used for heating, leaving the shells as solid waste. Currently, researchers are paying more attention to their industrial and medical uses. For example, Nie et al., (2019) used the shells to produce carbon-based materials. Xie et al., (2018) used shells to extract chemicals, including furfural, aldehydes, acids, and amine compounds, which can be applied to biomedical and biomaterial fields.

Liu et al., (2019b) studied the elimination of Cr(VI) and Cu(II) using *C. oleifera* nut shell and ethanol/NaOH-modified *C. oleifera* nut shell (MCONS), and found the removal efficiencies reached 16.39 and 27.26 mg/g for Cr(VI) and Cu(II) using MCONS, respectively, compared with 6.34 and 9.89 mg/g for *C. oleifera* nut shell. The difference may have been because the MCONS contained more carboxyl groups and had a higher surface area due to the modification with ethanol/NaOH.

1.3.3 Reduction method of graphene

However, as an adsorbent, the adsorption capacity of graphene remains limited when used directly due to the π - π and hydrophobic-hydrophobic interactions between its sheets (Agarwal and Zetterlund, 2021; Fadil et al., 2019). It leads to a large decrease in its surface area, which makes it easily agglomerate in aqueous solutions. Thus, researchers found that oxygen-containing hydrophilic groups on GO would provide more stability to improve the incorporation and uniform distribution by hindering the robust Van der Waals interactions between graphene sheets. rGO was found a promising adsorbent by removing oxygen-containing groups from GO while maintaining

the intrinsic properties of graphene and bypassing its disadvantages (Agarwal and Zetterlund, 2021; Dong et al., 2017; Shen et al., 2015; Shen and Chen, 2015; Thangavel and Venugopal, 2014; Velusamy et al., 2021; Wei et al., 2010). Many reduction methods have emerged with the development of science, such as adding reducing agents, high-temperature heat treatment, and electrochemical reduction, to obtain reduced graphene oxide (rGO).

1.3.3.1 Hydrazine reduction

Hydrazine was the earliest used reagent to reduce GO efficiently, among which hydrazine hydrate and phenyl hydrazine are most commonly put in use. The rGO from hydrazine reduction has good dispersion in aqueous solutions but has been limited in large-scale applications owing to its high cost and toxicity.

Ma et al., (2011) systematically studied the influence of reaction time on the reduction efficiency of oxygen-containing groups on GO by analyzing the chemical compositions and carbon atom contents of the reduction products. The results showed that the reduction process of GO mainly occurred in the first 1 h, with the total content of oxygen bonded carbon atoms decreasing from 83.6% to 22.1%, while there was only a 5.7% decrease in the following 23 h. This was because long reaction times would introduce C-N into rGO, causing hydrazine hydrate to attack C-O. From studying the mechanism of GO reduction at different temperatures, it can be concluded that increasing the temperature promoted the reduction process.

1.3.3.2 Electrochemical reduction method

In recent years, methods of preparing rGO through the electrochemical reduction of GO have been widely studied. Generally, the electrochemical reduction provides a simple, rapid, scalable, economical, and environmentally friendly way to produce high-quality rGO. However, it also has disadvantages, such as requiring the preparation of complex buffer solutions, high voltages to activate the process, and high air humidity (Zhou et al., 2009).

Deng et al., (2013) solved the above problems by using a glassy carbon electrode (GCE) to obtain electro-reduced graphene oxide (ERGO) via potentiostatic reduction of GO nanosheets falling off

in a single solution. Compared with the electrode modified by chemically reduced graphene oxide, the ERGO-modified electrode had a significantly improved voltametric response to L-tryptophan (TP) and L-tyrosine (Tyr), eliminated the interference from ascorbic acid and uric acid, and had good reproducibility. It can be used for the determination of TP and Tyr, with ranges of 0.2–40.0 and 0.5–80.0 $\mu\text{mol/L}$, respectively. The detection limits could be as low as 0.1 and 0.2 $\mu\text{mol/L}$.

1.3.3.3 Microwave reduction method

The "microwave" refers to electromagnetic waves with the frequency of 0.3–300 GHz. In a high-frequency alternating electric field, when the polarity of the medium is changed, the relative motion and friction between the molecules is intensified, which causes the heat generation in the medium to increase. This method possesses the advantages of a high efficiency and a high yield (gram level).

Chaban and Prezhdo, (2017) established the molecular reduction mechanism and the functional relationship between the time scale and the temperature through reactive molecular dynamics simulation experiments. The results showed that different oxygen-containing groups could be removed from GO at different temperatures, and products with different compositions could be produced, such as partially reduced rGO without carbonyl, hydroxyl, and carboxyl groups. The epoxy group was the most stable group in GO, which could be rearranged into carbonyl groups after rapid heating. The carbonyl group could prevent the formation of pores during the oxidation of graphite, making it difficult for the material to be reduced, and it would not damage the thermal stability and electronic properties of rGO. The edge oxygen-containing groups could not be removed by irradiation, but they had little effect on the performance of micron-level rGO chips. The oxygen-containing groups could be removed rapidly by microwave heating, and the rGO sheet was intact.

1.3.4 Application of reduced graphene oxide in environment

Hydrazine hydrate (N_2H_4) was usually taken as the reduction agent to prepare rGO from GO. However, this suffers high risks for environment and health resulting from the toxic and explosive

nature of N_2H_4 during the reduction step (Akhavan et al., 2012). It is crucial to find more environmentally friendly materials to reduce GO. Today, the application of extracts from plants for the green synthesis of rGO has been demonstrated to be eco-friendly and cost effective (Chettri et al., 2017; Khan et al., 2014; Sadhukhan et al., 2016). For example, Li et al., (2017) used eucalyptus leaf extract. Weng et al., (2019) studied green tea extract. Mahmudzadeh et al., (2019) used nettle extract, and Hou et al., (2016) used *Chrysanthemum* extract. The most useful components of plant extracts were two categories: i) polyphenols and ii) flavonoids (Agarwal and Zetterlund, 2021). Based on this method, some researchers focused on agricultural waste during the reduction process, which not only cut down the costs of reducing agents but also made use of the solid waste from agriculture activities, leading to better performances on waste-to-resource chains. Gan et al., (2019) studied the application of bagasse and its application in dye removal, which exhibited a high efficiency in the adsorption of dye. Zhao et al., (2020) studied the antibacterial effects of its saponins. For environmental applications, chitosan is usually selected as an adsorbent to obtain the goal of removing heavy metal ions. Liu et al., (2012) prepared a chitosan graphene composite (CSGO) through hydrogen bonding to remove Au(III) and Pb(II) from aqueous solution. The maximum adsorption amounts of Au(III) and Pb(II) reached 1076.65 and 216.92 mg/g, and the removal efficiency was still stable after three adsorption–desorption cycles. Lin et al., (2020) studied the adsorption behavior of Pb(II) by a nanomaterial, green tea extract–reduced graphene oxide (GT-RGO), which was found to be an environmentally friendly material that exhibited an excellent adsorption capacity for Pb(II) of 97.4% in an aqueous solution. The cycling experiment showed an 80.0% removal efficiency after four cycles, indicating the outstanding recyclability of this nanomaterial for Pb(II) removal.

1.3.5 Preparation of *C. oleifera* shell composite and its application in environment

C. oleifera shell (COS) is a by-product containing abundant amounts of various substances, including cellulose, phenols, terpenes, flavonoids, and polysaccharides. Most of them have been found to possess extensive biological properties, especially antioxidant properties (Luan et al., 2020; Wang et al., 2019). Various studies have been conducted on the comprehensive utilization of

COS in recent years, with most studies using COS to prepare biochar, activated carbon, or bio-adsorbents.

Yi et al., (2020) successfully synthesized a novel nitrogen-and phosphorus-enriched biochar (activated carbon, AC) nanomaterial through the co-pyrolysis of COS with ammonium polyphosphate (APP). The results showed a 72.4% removal efficiency of APP@AC-3 on Pb(II). This was much higher than that of unmodified AC, which was 26.4%. The study indicated that the co-pyrolysis of COSs and APP facilitated a better adsorption performance on the activated-carbon-based (biochar) material.

1.4 Information of this research

1.4.1 Research content

Graphene and other nanomaterials have many shortcomings during the traditional preparation process, such as the use of toxic and harmful chemicals prone to producing secondary pollution, cumbersome and complex preparation processes, and high costs. In order to avoid these problems, a green synthesis method was selected to prepare graphene materials in order to explore an environmentally friendly technology as well as improve the adsorption performances of pollutants in aquatic environments. Proanthocyanins and Tea saponin are the active ingredients in COS, with a strong antioxidant capacity, and they are an optimal deoxidizer for reducing graphene oxide in an environmentally friendly method (Tsukamoto et al., 1993; Ye et al., 2012). While there has been some success in applying COS for contaminant removal (Chaydarreh et al., 2021; H. Guo et al., 2018; Yi et al., 2020), research on the use of COS extract for reducing GO by an environmentally friendly way is still limited.

Response surface methodology (RSM), developed by Box and Wilson in 1951, is a multivariate statistical tool for optimizing experimental variables and responses (Bezerra et al., 2008). It can find the optimal reaction conditions by fitting the factors and response values using multiple quadratic regression equations. The process is on the basis of comprehensive analysis of experiments through a reasonable experimental design with a small number of experiments. This

method exhibits high experimental accuracy and good predictability, and it has been widely applied in the environmental field (Biglarijoo et al., 2016; Demim et al., 2014; Khobragade et al., 2016; Perez Mora et al., 2019; Zhang et al., 2017). RSM has three steps: i) select variables and design experiments, ii) set the response surface model and its evaluation based on empirical models from mathematical analysis, and iii) optimize the variables and responses. There are different RSM designs, and the central composite design (CCD) and Box–Behnken design (BBD) are commonly used (Al-Rashed, 2019; Priyadharshini and Bakthavatsalam, 2016). The CCD works better for experiments involving multi-factor and multi-level with continuous variables (typically more than five factors and three levels), while BBD is more applicable for experiments with fewer factors (generally fewer than five factors and three levels).

In this study, GO was reduced by COS extract through a green technology to prepare COS-rGO. The main objectives were to remove Cu(II) from an aqueous solution using COS-rGO and to propose the mechanism of Cu(II) removal. Based on the research background above, the contributions of this study are as follows:

i) COS-rGO was synthesized with COS extract as a reductant and coating agent through the BBD scheme of RSM, which provided a mathematical model of the interactions of independent variables in the COS-rGO preparation. The conditions of the COS-rGO preparation were determined by comparing the adsorption efficiency of Cu(II) in aqueous solutions.

ii) The COS-rGO material was applied to remove Cu(II) pollution in aqueous solutions. The effects on the removal efficiency under different conditions were explored by changing the experimental conditions, such as the dosage of COS-rGO, the initial concentration of Cu(II) solution, the pH value, and the reaction temperature. XRD, FT-IR, XPS, Raman spectroscopy, TEM, and other characterization methods were used to analyze the microstructures, surface morphologies, and chemical compositions of the COS-rGO before and after adsorbing Cu(II). The experimental data, adsorption isotherm model, adsorption kinetics and thermodynamics, and removal mechanism of Cu(II) by the COS-rGO were explored and analyzed.

iii) This study has demonstrated the prospects of reducing pollution using COS extract, which will be beneficial for environmental protection and the sustainable economic and agricultural development.

1.4.2 Innovation points

i) In this paper, COS extract was used as reducing agent and coating agent to reduce graphene oxide to make COS-rGO in an environmentally friendly way for the first time. Compared with using chemical reagents to synthesis nanomaterials, this method reduces the pollution caused by the use of toxic and harmful chemicals during the reduction process, and the method is simple and cheap to operate.

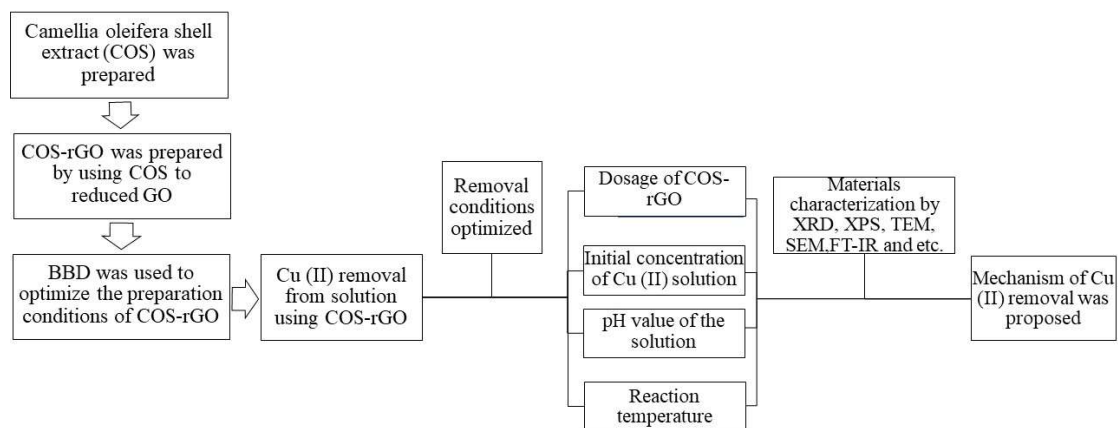
ii) The green synthesized nanomaterials (COS-rGO) were used to remove Cu(II) pollution in an aqueous environment. The effects of Cu(II) removal under different experimental conditions were investigated, and the adsorption mechanism was explored to provide technical support for removing heavy metal pollution in aqueous environments.

iii) A mathematical model (BBD) was used to design materials and validate the results through the designed experiments during the preparation process on the basic extract work from Jiang (2015), which made this research quicker and more accurate.

1.4.3 Technical route

For the experimental progress in this study, COS extract was firstly prepared with an environmentally friendly method, and then mixed with GO solution to prepare COS-rGO material by using BBD to optimize the experimental conditions. After that, the material was put into Cu(II) removal test and the removal experimental conditions were adjusted to find out the tendency towards better Cu(II) removal efficiencies. Besides, material characterization tests were conducted to study the removal mechanism of Cu(II) adsorption. The technical route of this study is as

follows:



2. Methodology

2.1 Materials and chemical reagents

Table 1 Materials and chemical reagents used in this experiment.

Name	Manufacturer	Grade
<i>Camellia oleifera</i> shell (COS)	Lishui, Zhejiang Province, China,	
Graphene oxide (GO)	Shanghai Macklin Biochemical Co. Ltd., China	Purity over 99%
Copper sulfate pentahydrate (CuSO ₄ · 5H ₂ O)	Aladdin Reagent Co. Ltd., Shanghai, China	Analytical grade
Anhydrous ethanol	Aladdin Reagent Co. Ltd., Shanghai, China	Analytical grade
Hydrochloric acid (HCl)	Shanghai Sinopharm Chemical Reagent Co., Ltd., China	Analytical grade

Note: i) COS was collected during the fruit ripening stage (October 2021); ii) ultrapure water was used during experiments.

2.2 Experimental instruments

Table 2 Instruments used in this experiment.

Instrument name	Manufacturer	Model
High-speed disintegrator	Yongkang Jiulan Hardware Products Co., Ltd., Zhejiang, China	Model 800A
Electric blender	Shanghai Meiyingpu Instrument Manufacturing Co., Ltd., China	JB90-S
Electronic balance	Mettler-Toledo Instruments (Shanghai) Co., Ltd.	LE201E/02
Ultrasonic cleaning	Kunshan Ultrasonic Instruments Co., Ltd	KQ218
Precision bath circulator	Ningbo Tianheng Instruments Co., Ltd.	THS-10
Circulating water multi-purpose vacuum pump	Henan Yuhua Instruments Co., Ltd.	SHZ-D (III)
Vacuum oven	Shanghai Sumsung Laboratory Instruments Co., Ltd.	DZG-6050
Atomic absorption spectrometer	Thermo Fisher Scientific Co., Ltd.	Thermo Fisher ICE3500
Laboratory bell-type common freeze dryer	Ningbo Scientz Biotechnology Co., Ltd., Zhejiang, China	SCIENTZ-10N/A
Refrigerated high-speed centrifuge	Thermo Fisher Scientific Co., Ltd.	Sorvall Stratos
Explosion proof refrigerator	Guangzhou Anfei Environmental Protection Technology Co., Ltd.	GYPEX BL-200SM100L
Water purification system	Merck Chemicals (Shanghai) Co., Ltd	Milli-Q Integral
Constant-temperature magnetic stirrer platform	JOANLAB Equipment CO., LTD	MHS4Pro

2.3 Preparation of COS extract

The COS extract (30 g) was crushed into fine powder through a high-speed disintegrator after discarding the rotted shells and drying the remaining shells at 60 °C in the oven for 3 h. The mixture of prepared COS powder (1g) and ultrapure water (14mL) in a beaker was stirred at 200 r/min by an electric blender and heated in a water bath at 80 °C for 3 h. The suspension was filtered through a sand core funnel with a 0.45- μm filter, and the filtrate resultant solution obtained was COS extract. After, the solution was put into a conical flask and placed in a refrigerator at a temperature of 4 °C for storage and further use.

2.4 Preparation of COS extract–reduced graphene oxide (COS-rGO)

The mixture of 1 L of ultrapure water and 0.5 g of GO was dispersed in an ultrasonic bath for 20 min, and COS extracts were added. Then mixture was heated in a water bath at 80 °C for 3 h (Jiang, 2015) following the filtration through a sand core funnel with a 0.45- μm filter. Solid products were obtained and washed with anhydrous ethanol and ultrapure water three times; then they were freeze-dried for 48 h through a vacuum freeze dryer. The final black solid product after drying was COS–reduced graphene oxide (COS-rGO).

2.5 Characterization

XRD: A D8 ADVANCE X-ray diffractometer (Cu K α) from the Bruker company in Germany was used in this experiment to study the crystalline phase structure changes from GO to COS-rGO through a reduction process under conditions with a voltage of 40 kV, current of 40 mA, and scanning range: $2\theta = 10^\circ\text{--}90^\circ$.

FT-IR: A NICOLET 6700 infrared analyzer from the Thermo Fisher Company in the United States was used in this experiment to measure the functional group changes of the COS-rGO. The samples were mixed and ground with 0.1% KBr (w/w); then they were pressed into thin discs and evaluated between the wavelength of 4000–400 cm^{-1} .

XPS: An AXIS SUPRA X-ray photoelectron spectrometer from the Kratos Company in the United Kingdom was used to analyze the distribution and speciation of elements on the surface of the COS-rGO. The excitation source was monochromatic Al K α X-ray ($h\nu = 1486.6$ eV) with power of 150 W.

Scanning electron microscopy (SEM): An S4800 scanning electron microscope from the Hitachi Company in Japan was used to analyze the changes of the morphology, structure, and elements of the COS-rGO material.

TEM: A JEM2100 transmission electron microscope from the Japan Electronics Corporation/Japan Technology Corporation in Japan was used to observe the micro-morphology and structure of the COS-rGO material at a 200-kV accelerating voltage.

Raman spectroscopy: Renishaw inVia Reflex confocal micro-Raman spectrometer from the Renishaw Company in the United States was used to study the structural components of the COS-rGO with a wavelength of 532 nm.

2.6 Pre-experiment of Cu(II) removal

A COS extract solution (30 g/L) and a GO solution (0.5 g/L) were mixed in the ratio of 1:5. The mixed suspension was placed in an 80°C water bath for 3 h (Jiang, 2015), after which it was filtered through a sand core funnel with a 0.45- μ m filter. Anhydrous ethanol and ultrapure water were used to wash the solid product three times, respectively. The solid COS-rGO product for the pre-experiment was obtained after drying in a vacuum freeze dryer for 48 h.

To compare the efficiencies of Cu(II) adsorption onto the different materials, experiments were conducted as follows. First, 50 mg of COS, GO, and COS-rGO were added to three beakers containing a 10 mg/L Cu(II) solution, and they were then placed on constant-temperature mixing platforms of the same model, with an operating speed of 200 rpm, reaction temperature of 20°C, and unadjusted pH (5.1). Samples were taken at selected time intervals of 5, 10, 30, 60, and 120 min using pipette guns and needle tubes with a 0.22- μ m filter membrane inside. The efficiencies

of the Cu(II) adsorbed by the COS, GO, and COS-rGO were investigated in duplicate and the residual Cu(II) concentration was determined by atomic absorption spectroscopy (AAS).

2.7 Design Experiment by Response Surface Methodology (RSM) to Prepare COS-rGO

The main factors of the preparation process of the COS-rGO were the duration of the reaction, extraction temperature, and ratio of COS and GO. However, the interaction between these factors still remained to be explored, and the optimization conditions could not be obtained quickly and accurately from experiments. To find the optimal conditions for preparing COS-rGO for Cu(II) adsorption, a Box–Behnken design (BBD), an important optimization analysis method of RSM, was implemented.

The three independent variables or factors (N) were the duration of the water bath (1–5 h), extraction temperature (70°C–90°C), and ratio of COS to GO (0.125–0.5), which were expressed by A, B, and C, respectively. The high, medium, and low levels of the independent variables were represented by 1, 0, and –1, respectively. Table 3 shows the variables and their different levels.

In this design, the BBD matrix of 17 experiments, including eight factorial points (2N), six axial points (2*N), and three central points (Cp), are given in Table 4. The COS-rGO samples were made according to the BBD matrix, and the removal efficiency of Cu(II) using these COS-rGO samples under the same conditions was compared to find the optimal condition for preparing COS-rGO. The results of the Cu(II) adsorption were evaluated using analysis of variance (ANOVA) and model graphics, including three-dimensional (3D) graphs, contour plots, and plots showing predicted vs. actual values.

The equation of model is as below:

$$Y = \beta_0 + \sum_{i=1}^k \beta_i X_i + \sum_{i=1}^k \sum_{j=1}^k \beta_{ij} X_i X_j + \sum_{i=1}^k \beta_{ii} X_i^2 + \varepsilon. \quad (2-1)$$

Y was the predicted response (Removal %); X_i and X_j were the coded values of the independent variables; β_0 was model constant; β_i , β_{ij} and β_{ii} were the regression coefficients for the linear,

quadratic and interaction terms, respectively; k was the number of independent variables and ε was the model residual error.

Table 3 Variables and their levels in Box–Behnken (BBD) of the experimental conditions for preparing COS-rGO.

Variables	Unit	Symbol	Levels		
			-1	0	1
Duration	h	A	1	3	5
Temperature	°C	B	70	80	90
Ratio of COS and GO	/	C	0.125	0.3125	0.5

Table 4 Box–Behnken (BBD) matrix of experimental conditions for preparing COS-rGO.

Run number	Variables		
	A	B	C
1	5	70	0.3125
2	3	80	0.3125
3	1	70	0.3125
4	3	80	0.3125
5	5	80	0.5
6	3	70	0.125
7	5	90	0.3125
8	3	90	0.5
9	1	90	0.3125
10	1	80	0.125
11	3	80	0.3125
12	3	80	0.3125
13	1	80	0.5
14	3	80	0.3125
15	3	90	0.125
16	5	80	0.125
17	3	70	0.5

2.8 Condition optimization of Cu(II) removal

To analyze the efficiency of Cu(II) removal by COS-rGO under various experimental conditions, a series of experiments were set up using different dosages of COS-rGO, initial concentrations of

the Cu(II) pollutant, pH values, and reaction temperatures. The adsorption kinetics and thermodynamics were analyzed to explore the mechanism of Cu(II) removal by COS-rGO. In order to reduce errors, all the experiments were conducted in parallel in two groups. The experimental steps were as follows:

i). To explore the effect of the dosage of COS-rGO on the removal efficiency, the dosages were set as 0.2, 0.5, and 1 g/L. Then, 0.02, 0.05, and 0.10 g of COS-rGO were added into beakers containing 100 mL of a Cu(II) solution with a concentration of 10 mg/L. The beakers were placed on constant-temperature mixing platforms of the same model, with an operating speed of 200 rpm, reaction temperature of 20 °C, and unadjusted pH (5.1).

ii). To explore the effect of the initial concentration of the Cu(II) solution on the removal efficiency, the initial concentrations were set as 5, 10, and 20 mg/L. Then, 0.05 g of COS-rGO was added into beakers containing 100 mL of Cu(II) solution with the same concentrations as above. The beakers were placed on the same model constant-temperature mixing platforms, with an operating speed of 200 rpm, reaction temperature of 20°C, and unadjusted pH (5.1).

iii). To explore the effect of the pH of the Cu(II) solution on the removal efficiency, the pH values were set as 1, 3, and 4. Then, 0.05 g of COS-rGO was added into beakers containing 100 mL of a Cu(II) solution with a concentration of 10 mg/L, and the pH values were adjusted as stated above. The beakers were placed on constant-temperature mixing platforms of the same model, with an operating speed of 200 rpm and reaction temperature of 20°C.

iv). To explore the effect of the reaction temperature of the Cu(II) solution on the removal efficiency, the temperature was set as 10°C, 20°C, and 30°C. Then, 0.05 g of COS-rGO was added into beakers containing 100 mL of Cu(II) solution with a concentration of 10 mg/L, and the temperatures were set as stated above. The beakers were placed on constant-temperature mixing platforms of the same model, with an operating speed of 200 rpm and an unadjusted pH (5.1).

The above samples were taken at selected time intervals of 5, 10, 30, 60, and 120 min using pipette guns and needle tubes with a 0.22- μ m filter membrane inside before testing, respectively.

The removal efficiencies of Cu(II) using COS-rGO were investigated, and the residual Cu(II) concentration was determined by AAS. The efficiency of Cu(II) removal using COS-rGO was calculated as followed equation:

$$R(\%) = \frac{C_0 - C_e}{C_0} \times 100\%. \quad (2-2)$$

R(%) was the removal efficiency of Cu(II), C_0 (mg/L) and C_e (mg/L) were the concentration of Cu(II) before adsorption and after t min, respectively.

2.9 Adsorbent regeneration and reuse experiments

To propose a better use of this adsorbent, the stability and recyclability were further studied. Desorption can be carried out by proton exchange using acids, by exchange with other ions (Mata et al., 2009). To test the applicability of COS-rGO, the same COS-rGO after desorption was reused for five times. In the desorption process, Cu(II)-loaded COS-rGO was placed in a 0.1 M HCl solution (pH of 1.1), stirred for 10 min, and then washed for three times with absolute ethanol, and ultrapure water, respectively. After being freeze-dried for 48 h, the COS-rGO could be reused to evaluate the adsorption capacity for Cu(II) under the same adsorption conditions.

3. Results and discussion

3.1 Removal results using different materials on Cu(II)

Experiments on the Cu(II) removal using different materials were conducted under the same conditions to compare the removal efficiencies. The initial concentration of the Cu(II) solution was set as 10 mg/L, the reaction temperature was 20 °C, and the dosage of adsorbent was 0.5 g/L. The Cu(II) removal efficiency by COS, GO, and COS-rGO, respectively, were compared without adjusting pH value. As shown in Figure 1, the adsorption of Cu(II) using GO (68.2%) and COS-rGO (84.7%) was noticeably higher than that using COS (38.1%). The reason that GO had a high removal efficiency was that the oxygen-containing groups on its surface worked. The reason that the adsorption efficiency of COS-rGO was higher than that of the GO was largely due to the reduction process from GO to COS-rGO, which lessened the aggregation of the GO material. Results from characterization of FT-IR and XPS confirmed that some biomolecules on the COS were partially coated on the rGO (Li et al., 2017), which caused an increase in the adsorption capacity of COS-rGO. Thus the adsorption sites on the COS-rGO promoted the removal efficiency (Qiu et al., 2018).

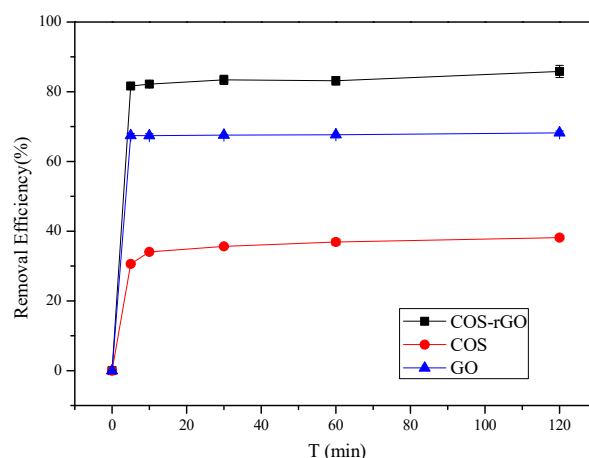


Figure 1 Adsorption of Cu(II) using different materials.

3.2 Results of Cu(II) removal by different COS-rGO samples according to Box–Behnken (BBD)

According to the BBD, batch experiments were conducted using the designed COS-rGO composites, and the adsorption results are shown in Table 5. The software Design-Expert v11 was used to perform quadratic regression fitting and variance analysis on the Cu(II) removal efficiency, and the results are shown in Table 6. The equation for this design is as below:

$$Y = 80.81 + 4.27A - 0.155B + 4.73C + 0.8AB + 1.25AC - 0.9BC - 9.18A^2 - 5.44B^2 - 6.89C^2. \quad (3-1)$$

Table 5 Adsorption results of Cu(II) by COS-rGO based on BBD.

Run number	Variables			Adsorption rate/% (2 h)
	A	B	C	
1	5	70	0.3125	71.00
2	3	80	0.3125	79.90
3	1	70	0.3125	62.01
4	3	80	0.3125	78.52
5	5	80	0.5	75.00
6	3	70	0.125	63.89
7	5	90	0.3125	72.00
8	3	90	0.5	71.29
9	1	90	0.3125	59.80
10	1	80	0.125	57
11	3	80	0.3125	80
12	3	80	0.3125	83.21
13	1	80	0.5	66
14	3	80	0.3125	82.44
15	3	90	0.125	65.67
16	5	80	0.125	61
17	3	70	0.5	73.11

Table 6 Analysis of variance (ANOVA) of quadratic model.

Source	Sum of squares	df	Mean square	F-value	p-value	
Model	1091.04	9	121.23	26.48	0.0001	significant
A-Duration	146.21	1	146.21	31.94	0.0008	
B-Temp	0.1922	1	0.1922	0.042	0.8435	
C-Ratio	178.98	1	178.98	39.1	0.0004	
AB	2.56	1	2.56	0.5593	0.4789	
AC	6.25	1	6.25	1.37	0.2809	
BC	3.24	1	3.24	0.7078	0.428	
A ²	354.6	1	354.6	77.47	< 0.0001	
B ²	124.47	1	124.47	27.19	0.0012	
C ²	199.71	1	199.71	43.63	0.0003	
Residual	32.04	7	4.58			
Lack of fit	16.9	3	5.63	1.49	0.3456	not significant
Pure error	15.15	4	3.79			
Cor total	1123.08	16				

NOTE: $R^2 = 0.9715$, $Adj-R^2 = 0.9348$, $Pre-R^2 = 0.7382$, coefficient of variation (C.V.) = 3.03%, Adequate precision = 14.5158, Cor is the abbreviation of Coefficient of Relationship

ANOVA is important for determining the accuracy of a quadratic model. Based on the results in Table 6, significant terms were identified for the model with an F-value of 26.48. P-values was 0.0001 means there was just 0.01% probability that an F-value this large would occur due to noise. Besides P-values less than 0.0500 suggested this model was highly significant, which was also consistent with the conclusion determined based on the F-value, that is, the model was significant. From this design, A, C, A², B², and C² were terms of significance. Values larger than 0.1000 meant that model terms were not significant. Therefore, the model was suitable for the process of COS-rGO preparation. The determination R² was 0.9715, indicating 97.15% of the response values could be simulated by this model. The coefficient of variation (C.V.) was 3.03%, which showed that the experiment had good accuracy and repeatability (Kainthola et al., 2019). The regression model equation can be used to analyze and predict the adsorption efficiency of Cu(II) using the COS-rGO material in this study. In addition, for the linear terms in the model, the duration (A) and ratio of COS/GO (C) were significant factors affecting the Cu(II) adsorption ($p < 0.05$). For the binomial terms, A² ($p < 0.0001$) had greater significance than C², indicating that the duration had

significant effect on the model. In addition, for the interaction between factors, AB, AC, and BC ($p > 0.05$) had no significant impacts on the model.

The predicted and actual values were plotted to judge the satisfactoriness of the model. As shown in the plots in Figure 2, the actual and predicted values were in close agreement, which signified that the model was suitable for use in preparing the COS-rGO.

In addition, a 3D response surface plot was generated based on the interactions between the independent variable factors, as shown in Figure 3. The interaction effects were illustrated by the duration (factor A) and the temperature (factor B) on the Cu(II) adsorption under the optimal ratio (factor C) (COS/GO was 0.3125). As the level of factor A changed from low to high, the response value first increased and then decreased, and there was a high response value range in the middle. Thus, the reaction time should be in the range of 2–4 h. The corresponding values changed slowly with the increase in the temperature, so the interaction effect of the two factors was not significant.

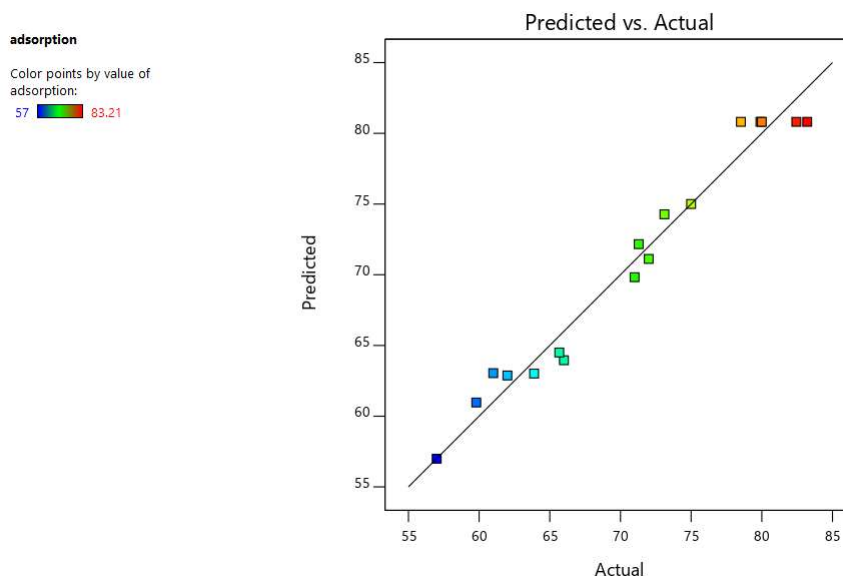


Figure 2 Experimental vs. predicted Cu(II) adsorption values.

Factor Coding: Actual

adsorption (%)

● Design points above predicted value

○ Design points below predicted value

57  83.21

X1 = A: Duration

X2 = B: Temp

Actual Factor

C: Ratio = 0.3125

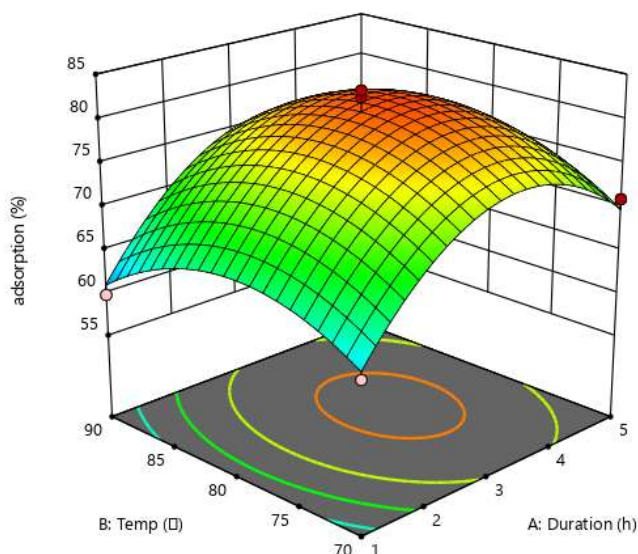


Figure 3 Surface plots illustrating Cu(II) adsorption influenced by operational factors.

3.3 Cu(II) removal by COS-rGO under different experimental conditions

3.3.1 Effect of dosage of COS-rGO on the Cu(II) removal efficiency

The efficiencies of Cu(II) removal by COS-rGO were 91.2%, 85.8%, and 45.1% when the dosages of COS-rGO were 1, 0.5, and 0.2 g/L, and approximately 5–10 min, the adsorption equilibrium was reached, as shown in Figure 5(a). The efficiency of Cu(II) removal increased from 45.1% to 85.8% when the dosage of COS-rGO increased from 0.2 to 0.5 g/l, mainly because of the enlargement of the contact area between Cu(II) and COS-rGO, creating more opportunities for contact between them, and the number of adsorption sites provided by COS-rGO also increased (Wang et al., 2014). Therefore, the removal efficiency was enhanced. With the progress of the reaction, the adsorption efficiency of Cu(II) was slightly different when the addition amounts of COS-rGO were 0.5 and 1.0 g/L. This was due to the gradual decrease in the Cu(II) concentration, and finally, it was almost completely removed, and the adsorption equilibrium was reached, which indicated that there was less effect from the increase in the adsorbent dosage on the reaction rate.

Besides, the Cu(II) removal efficiency did not reach 100% when the dosage of COS-rGO was 1.0 g/L, that may be caused by the enhancement of the aggregation of COS-rGO when the amount was increased from 0.5 to 1.0 g/L, leading to a decrease of the surface area and adsorption site, which resulted in the decrease of the adsorption efficiency of Cu(II) by COS-rGO.

3.3.2 Effect of the initial concentration of Cu(II) on the Cu(II) removal efficiency

As seen from Figure 5(b), the efficiencies of Cu(II) removal were 90.7%, 85.8%, 53.1%, and 21.1% when the initial concentrations of the Cu(II) solution were 5, 10, 20, and 40 mg/L. Increase of initial concentration of pollutants lead to a significant decrease of removal efficiency. The reason could be that when the concentration of Cu(II) was at a relatively low level, there were sufficient adsorption sites on the COS-rGO to ensure that Cu(II) was fully adsorbed. However, with the concentration of Cu(II) gradually increased, the adsorption sites provided by the COS-rGO remained limited. After reaching adsorption saturation, excessive Cu(II) in the solution could not be adsorbed, resulting in reduced removal efficiencies (Cheera et al., 2016).

3.3.3 Effect of the pH value of Cu(II) solution on the Cu(II) removal efficiency

Different pH values of the solution would bring changes to the surface charge and functional groups on the adsorbents, and they could also change the form of metal ions. Therefore, the pH value of solution played an obviously significant role during the adsorption process. In this paper, the pH ranged from 1 to 5.1. As seen in Figure 4(c), the removal efficiencies were 1.3%, 53.3%, 80.6%, and 85.8% when the pH values were 1, 3, 4, and 5.1 (unadjusted pH), respectively. As shown in Figure 4(c), as the pH value changed from 4 to 3, there was a large decrease of removal efficiency, from 80.6% to 53.3%. From the experimental results, lower pH levels led to a high H⁺ content. Hence, Cu(II) was electrostatically repelled by the positively charged functional groups, which to some extent prevented contact between Cu(II) and the COS-rGO, leading to a low Cu(II) removal efficiency (Cai et al., 2019). Furthermore, when the pH was not adjusted (5.1), the removal efficiency was 85.8%, which was only slightly different from the results at a pH of 4, suggesting that COS-rGO played an important role in Cu(II) adsorption in the pH range of 4–5.1.

3.3.4 Effect of reaction temperature on the Cu(II) removal efficiency

As observed in Figure 4(d), the temperature range of 20°C–40°C paid little influence on the removal efficiency. As the reaction temperature rose from 20°C to 40°C, there was a slight increase in the efficiency, from 85.8% to 90.6%. The increase in the removal rate with temperature suggested an increasing available active sites for adsorption with temperature, which indicated an endothermic process of removing Cu(II) by COS-rGO according to the calculation of Adsorption thermodynamics, where the high temperature promoted the adsorption and thus improved the removal efficiency (Song et al., 2017). Furthermore, the temperature increasing may lead to changes of the pore size, and to a relative increase in the diffusion of the Cu(II) owing to the decreasing of the solution viscosity, thus improving the exposure to the adsorption sites.

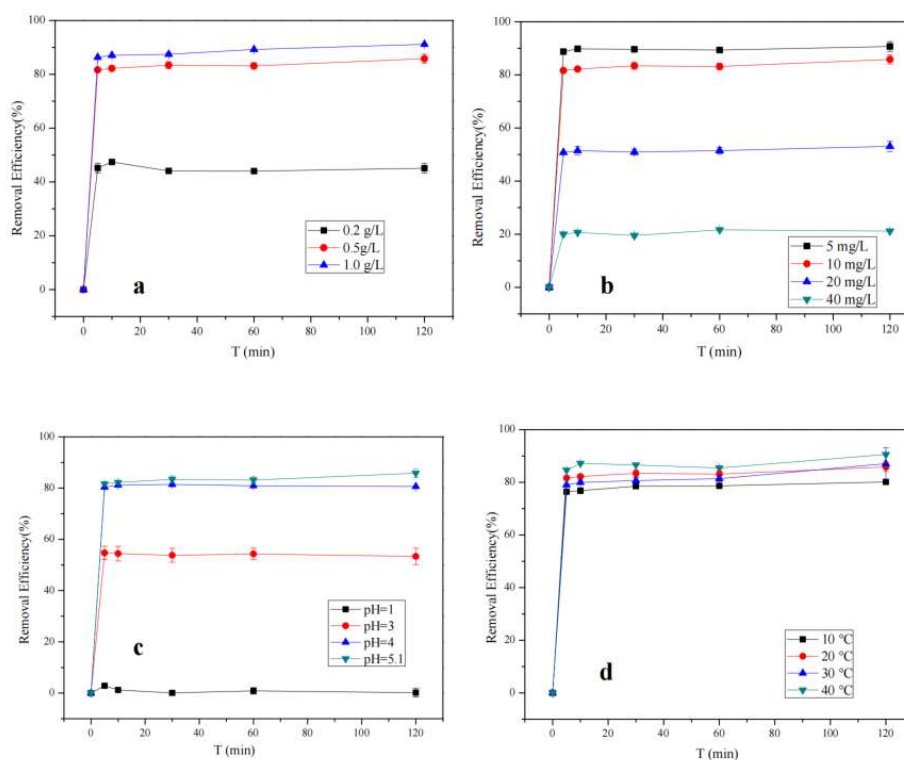


Figure 4 Efficiencies of Cu(II) removal by camellia oleifera shell–reduced graphene oxide (COS-rGO) under different conditions.

3.4 Characterization

3.4.1 XRD

The crystalline phase structure changes from GO to COS-rGO were examined using XRD, as seen in Figure 5. There was a sharp peak at $2\theta = 11.1^\circ$, corresponding to the diffraction of GO, and this diffraction peak disappeared for the COS-rGO, while a broad peak centered at $2\theta = 25.9^\circ$ appeared, corresponding to the characteristic diffraction of rGO (Chen et al., 2013; Zhang et al., 2010). The transmission of the diffraction peak at $2\theta = 11.1^\circ$ was attributed to the reduction process, confirming the successful reduction of GO to COS-rGO using the COS extract.

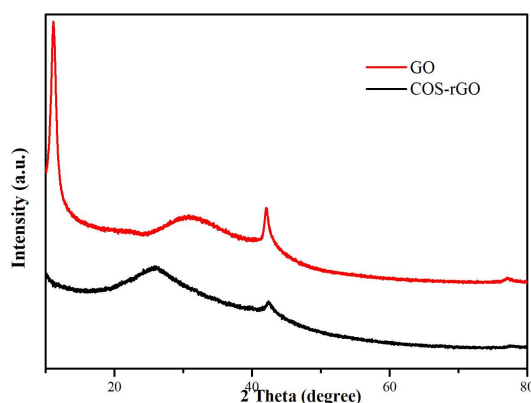


Figure 5 X-ray diffraction (XRD) patterns of graphene oxide and COS-rGO prepared with *Camellia oleifera* shell (COS).

3.4.2 SEM

The surface morphologies of the GO and COS-rGO were analyzed by SEM. From Figures 6 (a) and (b), there were many wrinkles and folded regions on the surfaces of the GO, revealing randomly aggregated, thin, crumpled-layer structures, which are a typical feature of graphene materials (Deng and Berry, 2016; Saleem et al., 2018). This was caused mainly by the coating of oxygen-containing groups, like carboxyl, epoxy, and hydroxyl groups, on the surface. Wrinkles and folds were observed on the surface of the COS-rGO, showing that the structure and surface morphology of GO were stable and the reduction process caused no destruction to the surface structures. The folded regions of COS-rGO are observed to be thinner than that on the surface of GO, which may be caused by reducing of the amount of oxygen-containing groups, and thus will give rise to the large specific surface area and make it easier to composite with Cu(II).

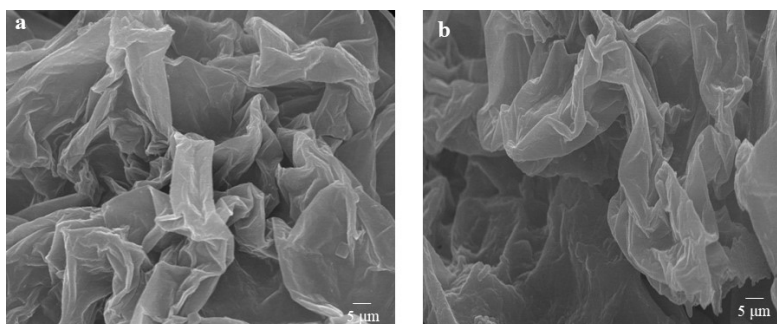


Figure 6 Scanning electron microscopy (SEM) images of (a) graphene oxide (GO) and (b) COS-rGO.

3.4.3 TEM

In order to further analyze the morphology of COS-rGO before and after exposure to Cu(II), TEM was used to examine the morphology and structure of the COS-rGO. As shown in Figure 7(a), there were a large number of crepe-like folds in the surface microstructure and irregular edges on the COS-rGO, as well as a slight stacking which can be caused by van der Waals forces during the formation (Chamoli et al., 2016). As shown in Figure 7(b), many spherical particles adhered to the surface of the COS-rGO, corresponding to the results from XPS, which meant that Cu(II) ions were arrayed on the surface of the graphene sheets and they did not aggregate and stood isolated from each other on the surface, covering a large area of the COS-rGO sheets. Besides, it can be seen that not all the Cu(II) ions were spherical, which may be due to the partial oxidation of Cu(II) in air (Kichukova et al., 2022).

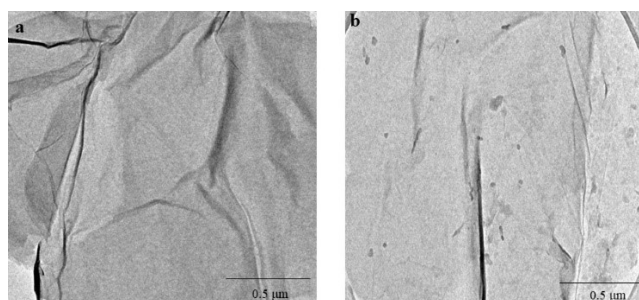


Figure 7 Transmission electron microscopy (TEM) images of COS-rGO (a) before and (b) after exposure of Cu(II).

3.4.4 FT-IR

The FT-IR spectra of COS, GO, and COS-rGO are presented in Figure 8. The broad peak centered at $\sim 3410\text{ cm}^{-1}$ was attributed to the stretching vibrations of -OH generated by adsorbed water. Double peaks appearing at 1720 and 1611 cm^{-1} were attributed to -C=O and C-C stretching bands (Emiru and Ayele, 2017). Compared with GO, three characteristic peaks ascribed to COS appeared in the rGO: -CH₂/CH₃ at 1354 cm^{-1} , -C-O at 1237 cm^{-1} , and -CH at 762 cm^{-1} , which suggested that the biomolecules of the COS could be wrapped around the surfaces of the GO.

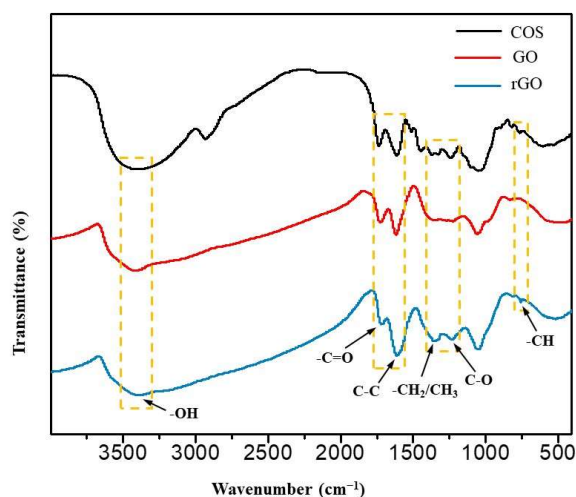


Figure 8 Fourier-transform infrared spectroscopy (FT-IR) spectra of COS, GO, and COS-rGO.

3.4.5 Raman spectroscopy

Raman spectra provides more insights into the structural changes and type of defects of the materials. The Figure 9 showed two intensive bands in the range from 1100 to 1700 cm^{-1} where the characteristic peaks at 1345 and 1589 cm^{-1} could be the D and G bands, respectively, which were characteristic for graphite materials. The intensity of the G band reflected the thickness of the stacked graphene sheets while the width related to the deformation and strain in the graphene sheets. The D-band was raised from the presence of disorder, edges and defects of the graphene sheets. In this study, the D peak of GO The D peak at 1345 cm^{-1} was caused by the in-plane tensile vibrations of the sp²-hybridized carbon atoms, while the G peak at 1589 cm^{-1} represented defects of the carbon atom lattice. The intensity ratio of the D peak to the G peak, denoted as i_D/i_G , is usually used to determine graphene's defect degree (T. Guo et al., 2018). The i_D/i_G of the GO

and the COS-rGO were 0.90 and 1.01, respectively. The I_D/I_G value of COS-rGO was higher than that of GO, showing a successful reduction from GO to COS-rGO using the COS extract (Li et al., 2018). During the synthesis process, the hydroxyl, carboxyl, and other functional groups on GO were removed, which also provided more active adsorption sites for adsorbing Cu(II) in the solution.

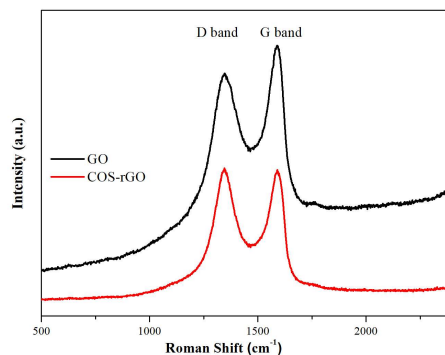


Figure 9 Raman spectra of GO and COS-rGO.

3.4.6 XPS

XPS can determine the elemental contents in the material (except H and He). The C1s peak represented a superposition of lines, corresponding to different C-bonds. Through the analysis of COS-rGO by XPS, the adsorption process of Cu(II) by COS-rGO was further explored. From Figures 8(a), 8(c), and 8(d), there were two obvious signals of the C 1s spectrum on the COS-rGO, which were attributed to hydroxyl groups (C-OR 285.0 eV) and aromatic carbon groups (CH_x, C-C/C=C 283.1 eV) (Xie et al., 2019), which were typical of rGO materials. These functional groups were derived from the COS extract, which confirmed the successful synthesis of COS-rGO using the COS extract. Figure 8(b) shows the XPS fitting results of Cu after the COS-rGO adsorbed Cu(II). The characteristic peaks in the figure corresponded to Cu 2p_{1/2} (933.4 eV) and Cu 2p_{3/2} (954.0 eV), which confirmed a successful adsorption of Cu(II) on the COS-rGO. Regarding the spectrum of Cu 2p_{3/2} (954.0 eV), binding energy greater than 934.4 eV can be attributed to the oxidation of Cu(II) in air. That confirmed to the observation in TEM, and suggested a solid chemical bond during the adsorption process (Severino et al., 1998). From Figure 8(c), the characteristic peaks including C=O, C-O, and C-OH bonds were present, which may be a result of the biomolecules wrapping around the surfaces of the COS-rGO from the COS extract (Li et al.,

2017; Lin and Chen, 2014).

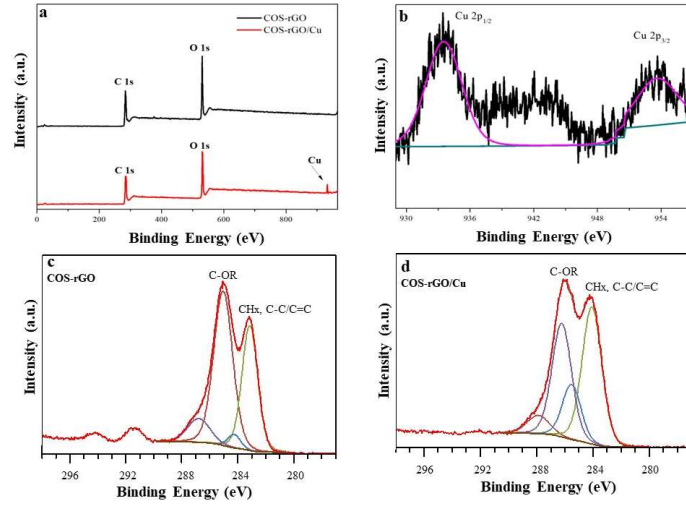


Figure 10 (a) X-ray photoelectron spectroscopy (XPS) survey spectra of COS-rGO before and after exposure to Cu(II). (b) Cu 2p spectrum of COS-rGO after adsorption of Cu(II). C 1s spectrum of COS-rGO (c) before and (d) after adsorption of Cu(II).

3.5 Adsorption kinetics

To study the mechanism of Cu(II) adsorption using COS-rGO, models of the pseudo-first-order and pseudo-second-order kinetics were fitted. The pseudo-first-order kinetics model, which assumes that the diffusion rates are primarily responsible for controlling the adsorption process, is as below:

$$\ln(q_e - q_t) = \ln q_e - k_1 t. \quad (3-2)$$

The pseudo-second-order kinetics model, which assumes that the unoccupied adsorption vacancies on the adsorbent surface are responsible for the rate during adsorption process, is expressed as follows:

$$\frac{t}{q_t} = \frac{1}{k_2 q_e^2} + \frac{t}{q_e}. \quad (3-3)$$

q_t (mg/g) and q_e (mg/g) were the amount of Cu(II) adsorption at t time and at equilibrium. k_1 and k_2 were the constant of pseudo-first-order kinetics model and pseudo-second-order kinetics model.

R^2 was the correlation coefficient, which was considered as the standard to determine the conformity of the results. R^2 was considered as the standard to determine the conformity of the results.

The results of two kinetics models were calculated based on data in Figure 4, and listed in Table 7. The R^2 values of pseudo-first-order kinetics model were far less than that of the pseudo-second-order kinetics model and the theoretical adsorption amounts calculated by the pseudo-first-order kinetics model were quite different from actual amounts at equilibrium. While from the data of the pseudo-second-order kinetics model, R^2 values ≥ 0.999 , and the theoretical adsorption capacities were more close to actual values at equilibrium, which meant it was more consistent with the adsorption process, indicating that chemical adsorption was the primary control step during the adsorption (Zhang et al., 2018). With an increasing from 283 to 313 K of the temperature, k_2 decreased significantly, indicating a decrease in the reaction rate. Furthermore, a decrease in the removal efficiency indicated that the removal of Cu(II) by COS-rGO was a process controlled by the reaction rate (T. Guo et al., 2018).

Table 7 Kinetics parameters for Cu(II) removal by COS-rGO.

Temperature (K)	Pseudo-first-order			Pseudo-second-order		
	k_1 (1/min)	q_{e1} (mg/g)	R^2	k_2 (g/(mg·min))	q_{e2} (mg/g)	R^2
283	0.0019	0.540	0.0297	0.0985	17.544	0.9999
293	0.0033	1.055	0.1006	0.0556	19.646	0.9998
313	0.0027	1.194	0.3064	0.0444	17.065	0.9995

Based on the Arrhenius formula, the activation energy E_a was calculated to further explore the relationship between the chemical reaction rate and temperature. The Arrhenius formula is as follows:

$$\ln K_2 = \ln A - \frac{E_a}{RT}. \quad (3-4)$$

K_2 (g/(mg·min)) was the constant of pseudo-second-order kinetics model. E_a (kJ/mol) was the activation energy. A was the constant of Arrhenius. R (J/K·mol) was the constant of Molar gas (8.314). T (K) was the absolute temperature.

3.6 Adsorption isotherms

Through data fitting, the adsorption isotherm model of Cu(II) removal by the COS-rGO was studied to further explore the interactions between COS-rGO and the pollutant. The initial concentration of Cu(II) was set in the range of 1–50 mg/L, and batch experiments were conducted. An isothermal adsorption model was used to further investigate the reaction process. The data of the Cu(II) adsorption by COS-rGO was analyzed by Langmuir and Freundlich models and Table 8 showed the results.

The Langmuir adsorption isotherm model, which assumes that the adsorption process is a monolayer adsorption occurring on the surface of the adsorbent, is expressed in the following equation:

$$\frac{C_e}{q_e} = \frac{C_e}{q_0} + \frac{1}{q_0 K_L}. \quad (3-5)$$

K_L was the constant of Langmuir. C_e (mg/L) was the Cu(II) concentration at equilibrium in solution. q_e (mg/g) and q_0 (mg/g) were the adsorption amount of Cu(II) at equilibrium and theoretical maximum adsorption amount, respectively.

The Freundlich adsorption isotherm model, which assumes that there are unbalanced adsorption sites with multi-layer adsorption, is expressed in the following equation:

$$\ln q_e = \ln K_F + \frac{1}{n} \ln C_e. \quad (3-6)$$

K_F (mg/g) was the binding energy constant, which reflects the adsorption capacity of the adsorbate on heavy metals (Cheng et al., 2022), n was the Freundlich constant. C_e (mg/L) was the Cu(II) concentration at equilibrium in solution. q_e (mg/g) was the adsorption amount of Cu(II) at equilibrium.

The Temkin adsorption isotherm model, which assumes that an increase in the adsorption capacity will lead to a linear decrease in the adsorption heat, rather than a logarithmic decrease (Sharma et al., 2018), is expressed in the following equation:

$$q_e = B(\ln C_e) + B(\ln A). \quad (3-7)$$

q_e (mg/g) is the adsorption amount at adsorption equilibrium. C_e (mg/L) is the Cu(II) concentration in solution at equilibrium. B is the constant related to adsorption heat. A (L/g) is the maximum binding energy at equilibrium.

From Table 8, the experimental results of Cu(II) adsorbed by the COS-rGO were best captured by the Langmuir adsorption isotherm model based on the R^2 values from the three different adsorption isotherm models. Data from the Langmuir model showed the adsorption capacity at equilibrium was closer to the theoretical amount, which meant the removal performance of Cu(II) using the COS-rGO was primarily based on spontaneous chemical adsorption (Huang et al., 2014). Thus, conclusion came as that the adsorption process of Cu(II) was based on uniform monolayer adsorption behavior on the material surface and identical adsorption sites, which might have resulted from the interaction between p-p bonds on the adsorbent (Akpotu and Moodley, 2018).

Table 8 Isotherm parameters for Cu(II) removal by COS-rGO.

Temperature (K)	Freundlich			Langmuir			Temkin		
	n	K_F (mg/g)	R^2	Q_m (mg/g)	K_L (L/mg)	R^2	A (L/g)	B	R^2
283	3.76	8.19	0.7912	14.49	2.95	0.9932	0.52	7.50	0.9278
293	3.67	8.96	0.8011	16.23	7.42	0.9872	0.48	8.18	0.918
313	3.50	10.11	0.8174	18.15	2.80	0.9924	0.45	8.97	0.9157

3.7 Adsorption thermodynamics

The thermodynamic parameters were evaluated through the removal efficiencies of Cu(II) adsorbed by the COS-rGO at different temperatures. The formulas are as follows:

$$\ln\left(\frac{q_e}{C_e}\right) = \frac{\Delta S^0}{R} - \frac{\Delta H^0}{RT}, \quad (3-8)$$

$$\frac{q_e}{C_e} = K, \quad (3-9)$$

$$\Delta G^0 = -RT \ln K. \quad (3-10)$$

q_e (mg/g) is the adsorption amount of Cu(II) at equilibrium. C_e (mg/L) is the Cu(II) concentration in solution at equilibrium. K was the equilibrium coefficient. R was the constant of gas (8.314 J mol/K). T (K) was the reaction temperature. ΔG^0 (kJ/mol) was Gibbs free energy, ΔS^0 (kJ/mol) was entropy change, ΔH^0 (kJ/mol) was enthalpy change and the values of ΔS^0 and ΔH^0 are calculated by the intercept and slope of the linear fitting of $\ln q_e/C_e$ to $1/T$.

The thermodynamic parameters were calculated based on data in Figure 4, and Table 9 shows the values of ΔG , ΔH , and ΔS at different temperatures. From Table 9, $\Delta H^0 > 0$ indicated that this adsorption was endothermic which was in accordance with the results of temperature experiments. The value of $\Delta S^0 > 0$ indicated an increase in the randomness on the interface between the solid and solution as the reaction progressed. Under different temperatures, all the values of $\Delta G^0 < 0$ indicated that the adsorption process was a spontaneous reaction, and the values of ΔG^0 ranging from -20 to 80 kJ/mol illustrated that the adsorption process involved the cooccurrence of chemical and physical adsorption (Chang et al., 2021).

Table 9 Thermodynamic parameters for Cu(II) adsorption using COS-rGO.

ΔH^0 (kJ/mol)	ΔS^0 (kJ/mol)	ΔG^0 (kJ/mol)		
		283 K	293 K	313 K
21.00	0.086	-3.28	-4.38	-5.90

3.8 Mechanism of Cu(II) removal using COS-rGO

The heavy metal ions removal from aqueous solutions by COS-rGO was dominated by various mechanisms, such as complex formation, electrostatic interaction, ion-exchange, precipitation and reduction (Fan et al., 2017). The XPS scan spectrum of COS-rGO/Cu indicated the existence of carbon, oxygen and iron. The Langmuir equation showed a better agreement with equilibrium isotherm data. COS-rGO followed kinetic data well while the thermodynamic calculation revealed that Cu(II) adsorption was feasible, spontaneous and endothermic in nature. The enthalpy change (21.00 kJ/mol) indicated that chemisorption was mainly responsible for Cu(II) adsorption while

the positive value of entropy revealed the increase in irregularity or randomness at the water-solid interface during adsorption onto this substrate. Thus, based on the experiments and analysis results discussed above, a potential mechanism of Cu(II) removal using COS-rGO was proposed. As shown in Figure 11, the removal process mainly occurred through chemical adsorption, which involved i) the unique adsorption properties of graphene materials for metal ions, such as the reaction between Cu(II) ions and electrons on the π -bonds, and ii) Cu(II) ions were adsorbed on the COS-rGO by functional groups loaded on its surface due to the strong interaction between functional groups (eg. C=O and C-N) of COS-rGO and Cu(II) (Zhang et al., 2014), which provides lots of adsorption sites for removal of Cu(II).

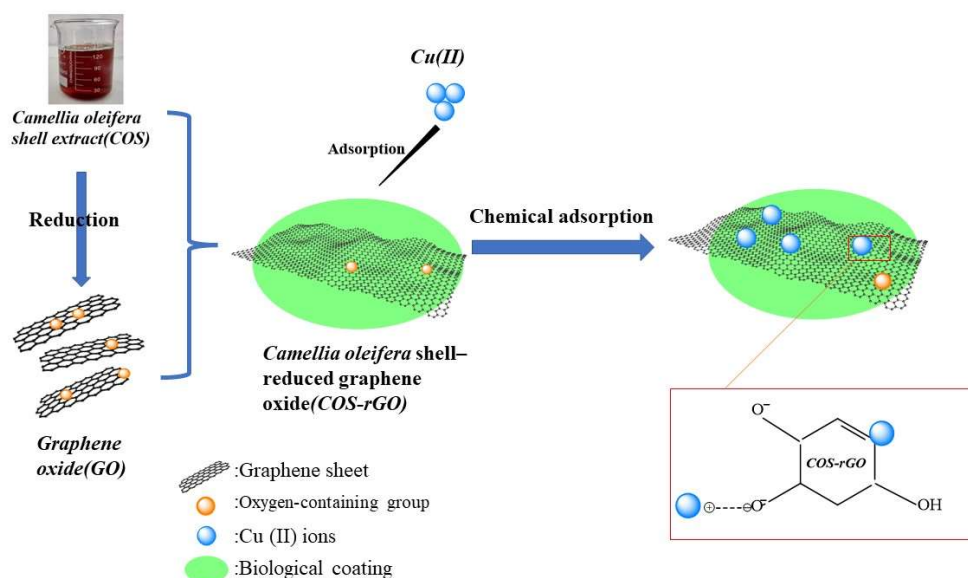


Figure 11 Proposed mechanisms of Cu(II) removal by COS-rGO.

3.9 Recyclability and stability studies

The recyclability of adsorbents is an important standard to evaluate the value and competitiveness of adsorbents. Desorption can be carried out by proton exchange using acids, by exchange with other ions (Mata et al., 2009). To test the applicability of COS-rGO, 0.1 M HCl, absolute ethanol, and ultrapure water were used to clean the adsorbed COS-rGO, respectively, to study the recycling performance. First, 100 mL of 10 mg/L Cu(II) solution and 50 mg of COS-rGO were stirred on a

constant-temperature mixing platform at 200 r/min and 20°C for 120 min. Then, the sample was centrifuged and filtered to obtain the supernatant. The residual Cu(II) concentrations were analyzed by AAS. Then, 0.1 M HCl, absolute ethanol, and ultrapure water were used to wash the COS-rGO three times, respectively. After that, 100 mL of Cu(II) was added again. The above steps were repeated for five times using the same COS-rGO, and adsorption results are shown in Figure 12. There was a 57.6% removal efficiency at the fifth cycle, indicating that the COS-rGO exhibited a great recyclability for Cu(II) removal (Chang et al., 2021; Li et al., 2019).

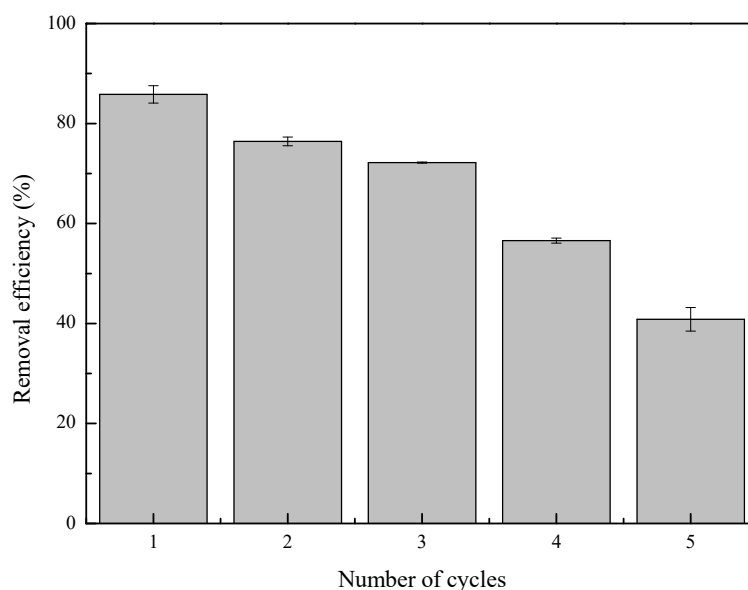


Figure 12 COS-rGO recycling experiment.

4. Conclusions and prospects

4.1 Conclusions

In this thesis, COS-rGO adsorbents were synthesized by reducing GO with COS extracts based on an environmentally friendly method for the first time, and the prepared COS-rGO was successfully applied to remove Cu(II) from the aqueous solution. The BBD was used for optimizing the experimental condition in a more effective way. The influence of various experimental conditions on removal efficiency were evaluated and optimized. Also, the kinetic and thermodynamic studies for Cu(II) adsorption on COS-rGO were investigated. And the mechanism on the adsorption of Cu(II) to COS-rGO was proposed based on the results of characterization of prepared COS-rGO and adsorption experimental results. The conclusions are as follows:

- i) From the adsorption isotherms, kinetics models, and thermodynamic models, it was concluded that the adsorption process of Cu(II) by COS-rGO followed a pseudo-second-order kinetics process as a spontaneous endothermic reaction, and a higher temperature was conducive to the adsorption process.
- ii) According to the results of characterization by using Fourier-transform infrared spectroscopy (FT-IR), scanning electron microscopy (SEM), transmission electron microscopy (TEM), and X-ray diffraction (XRD), it was confirmed that the removal of Cu(II) by COS-rGO was a result of chemical adsorption following a rate-controlled process and Langmuir model was applied to this adsorption process.
- iii) The batch experimental results showed that the good stabilization and dispersion of COS-rGO provide a short time for the contact between adsorption sites and Cu(II). Besides, the recycling experiment of COS-rGO indicated a good recyclability of the absorbent where a 57.6% removal rate of Cu(II) can be achieved by the same COS-rGO after five cycles. These results indicate that the COS-rGO has good adsorption efficiency and reutilization during the Cu(II) removal, which is very important for wastewater treatment.

4.2 Prospects

Follow-up work to this study should also be considered:

i) The process of reducing graphene oxide remains to be explored more deeply to determine the most effective substances in COS extract and to understand the interactions between these substances during the reduction period. Besides, the adsorption experiment for complex pollutants in aquatic environment can be developed to get an improvement for its utilization in industrial field, as there are more complex contaminants in the wastewater.

ii) Due to the good desorption ability and recyclability of COS-rGO, more researches can be further developed into the metal recycling field. The valuable metal ions can be adsorbed by the absorbent from low concentration and then desorbed to accumulate into a high concentrated solution, thus to achieve the goal of metal recycling.

Bibliography

1. Aboul-Magd, A.-A.S., Al-Husain, S.A.-R., Al-Zahrani, S.A., 2016. Batch adsorptive removal of Fe(III), Cu(II) and Zn(II) ions in aqueous and aqueous organic–HCl media by Dowex HYRW₂-Na Polisher resin as adsorbents. *Arab. J. Chem.* 9, S1–S8. <https://doi.org/10.1016/j.arabjc.2011.04.002>
2. Agarwal, V., Zetterlund, P.B., 2021. Strategies for reduction of graphene oxide – A comprehensive review. *Chem. Eng. J.* 405, 127018. <https://doi.org/10.1016/j.cej.2020.127018>
3. Akhavan, O., Kalaei, M., Alavi, Z.S., Ghiasi, S.M.A., Esfandiari, A., 2012. Increasing the antioxidant activity of green tea polyphenols in the presence of iron for the reduction of graphene oxide. *Carbon* 50, 3015–3025. <https://doi.org/10.1016/j.carbon.2012.02.087>
4. Akpotu, S.O., Moodley, B., 2018. Application of as-synthesised MCM-41 and MCM-41 wrapped with reduced graphene oxide/graphene oxide in the remediation of acetaminophen and aspirin from aqueous system. *J. Environ. Manage.* 209, 205–215. <https://doi.org/10.1016/j.jenvman.2017.12.037>
5. Almasian, A., Giahhi, M., Chizari Fard, Gh., Dehdast, S.A., Maleknia, L., 2018. Removal of heavy metal ions by modified PAN/PANI-nylon core-shell nanofibers membrane: Filtration performance, antifouling and regeneration behavior. *Chem. Eng. J.* 351, 1166–1178. <https://doi.org/10.1016/j.cej.2018.06.127>
6. Al-Rashed, A.A.A.A., 2019. Optimization of heat transfer and pressure drop of nano-antifreeze using statistical method of response surface methodology. *Phys. Stat. Mech. Its Appl.* 521, 531–542. <https://doi.org/10.1016/j.physa.2019.01.095>
7. Alyüz, B., Veli, S., 2009. Kinetics and equilibrium studies for the removal of nickel and zinc from aqueous solutions by ion exchange resins. *J. Hazard. Mater.* 167, 482–488. <https://doi.org/10.1016/j.jhazmat.2009.01.006>
8. Anwer, M., Bushra, A., 2015. *Aspergillus niger*-a novel heavy metal bio-absorbent and pesticide tolerant fungus. *Res. J. Chem. Environ.* 19(2), 57–66.
9. Bashir, A., Malik, L.A., Ahad, S., Manzoor, T., Bhat, M.A., Dar, G.N., Pandith, A.H., 2019. Removal of heavy metal ions from aqueous system by ion-exchange and biosorption methods. *Environ. Chem. Lett.* 17, 729–754. <https://doi.org/10.1007/s10311-018-00828-y>
10. Bezerra, M.A., Santelli, R.E., Oliveira, E.P., Villar, L.S., Escaleira, L.A., 2008. Response surface methodology (RSM) as a tool for optimization in analytical chemistry. *Talanta* 76, 965–977. <https://doi.org/10.1016/j.talanta.2008.05.019>
11. Biglarijoo, N., Mirbagheri, S.A., Ehteshami, M., Ghaznavi, S.M., 2016. Optimization of Fenton process using response surface methodology and analytic hierarchy process for landfill leachate treatment. *Process Saf. Environ. Prot.* 104, 150–160. <https://doi.org/10.1016/j.psep.2016.08.019>
12. Bilal, M., Ihsanullah, I., Younas, M., Ul Hassan Shah, M., 2021. Recent advances in applications of low-cost adsorbents for the removal of heavy metals from water: A critical review. *Sep. Purif. Technol.* 278, 119510. <https://doi.org/10.1016/j.seppur.2021.119510>
13. Cai, W., Weng, X., Chen, Z., 2019. Highly efficient removal of antibiotic rifampicin from aqueous solution using green synthesis of recyclable nano-Fe₃O₄. *Environ. Pollut.* 247, 839–846. <https://doi.org/10.1016/j.envpol.2019.01.108>

14. Chakravarty, S., Mohanty, A., Sudha, T.N., Upadhyay, A.K., Konar, J., Sircar, J.K., Madhukar, A., Gupta, K.K., 2010. Removal of Pb(II) ions from aqueous solution by adsorption using bael leaves (*Aegle marmelos*). *J. Hazard. Mater.* 173, 502–509. <https://doi.org/10.1016/j.jhazmat.2009.08.113>
15. Chamoli, P., Sharma, R., K. Das, M., K. Kar, K., 2016. *Mangifera indica*, *Ficus religiosa* and *Polyalthia longifolia leaf* extract-assisted green synthesis of graphene for transparent highly conductive film. *RSC Adv.* 6, 96355–96366. <https://doi.org/10.1039/C6RA19111H>
16. Chang, L., Pu, Y., Jing, P., Cui, Y., Zhang, G., Xu, S., Cao, B., Guo, J., Chen, F., Qiao, C., 2021. Magnetic core-shell MnFe₂O₄@TiO₂ nanoparticles decorated on reduced graphene oxide as a novel adsorbent for the removal of ciprofloxacin and Cu(II) from water. *Appl. Surf. Sci.* 541, 148400. <https://doi.org/10.1016/j.apsusc.2020.148400>
17. Chaydarreh, K.C., Lin, X., Guan, L., Yun, H., Gu, J., Hu, C., 2021. Utilization of tea oil camellia (*Camellia oleifera* Abel.) shells as alternative raw materials for manufacturing particleboard. *Ind. Crops Prod.* 161, 113221. <https://doi.org/10.1016/j.indcrop.2020.113221>
18. Cheera, P., Karlapudi, S., Sellola, G., Ponneri, V., 2016. A facile green synthesis of spherical Fe₃O₄ magnetic nanoparticles and their effect on degradation of methylene blue in aqueous solution. *J. Mol. Liq.* 221, 993–998. <https://doi.org/10.1016/j.molliq.2016.06.006>
19. Chen, H., Li, J., Wu, X., Wang, X., 2014. Synthesis of Alumina-Modified Cigarette Soot Carbon As an Adsorbent for Efficient Arsenate Removal. *Ind. Eng. Chem. Res.* 53, 16051–16060. <https://doi.org/10.1021/ie503057g>
20. Chen, J., Yao, B., Li, C., Shi, G., 2013. An improved Hummers method for eco-friendly synthesis of graphene oxide. *Carbon* 64, 225–229. <https://doi.org/10.1016/j.carbon.2013.07.055>
21. Chen, Q., Luo, Z., Hills, C., Xue, G., Tyrer, M., 2009. Precipitation of heavy metals from wastewater using simulated flue gas: Sequent additions of fly ash, lime and carbon dioxide. *Water Res.* 43, 2605–2614. <https://doi.org/10.1016/j.watres.2009.03.007>
22. Chen, Q., Yao, Y., Li, X., Lu, J., Zhou, J., Huang, Z., 2018. Comparison of heavy metal removals from aqueous solutions by chemical precipitation and characteristics of precipitates. *J. Water Process Eng.* 26, 289–300. <https://doi.org/10.1016/j.jwpe.2018.11.003>
23. Cheng, M., Yao, C., Su, Y., Liu, J., Xu, L., Bu, J., Wang, H., Hou, S., 2022. Cyclodextrin Modified Graphene Membrane for Highly Selective Adsorption of Organic Dyes and Copper (II) Ions. *Eng. Sci.* 299–307. <https://doi.org/10.30919/es8d603>
24. Chettri, P., Vendamani, V.S., Tripathi, A., Singh, M.K., Pathak, A.P., Tiwari, A., 2017. Green synthesis of silver nanoparticle-reduced graphene oxide using *Psidium guajava* and its application in SERS for the detection of methylene blue. *Appl. Surf. Sci.* 406, 312–318. <https://doi.org/10.1016/j.apsusc.2017.02.073>
25. Dayana Priyadharshini, S., Bakthavatsalam, A.K., 2016. Optimization of phenol degradation by the microalga *Chlorella pyrenoidosa* using Plackett–Burman Design and Response Surface Methodology. *Bioresour. Technol.* 207, 150–156. <https://doi.org/10.1016/j.biortech.2016.01.138>
26. Demim, S., Drouiche, N., Aouabed, A., Benayad, T., Couderchet, M., Semsari, S., 2014. Study of heavy metal removal from heavy metal mixture using the CCD method. *J. Ind. Eng. Chem.* 20, 512–520. <https://doi.org/10.1016/j.jiec.2013.05.010>
27. Demopoulos, G.P., 2009. Aqueous precipitation and crystallization for the production of

- particulate solids with desired properties. *Hydrometallurgy* 96, 199–214. <https://doi.org/10.1016/j.hydromet.2008.10.004>
28. Deng, K.-Q., Zhou, J., Li, X.-F., 2013. Direct electrochemical reduction of graphene oxide and its application to determination of L-tryptophan and L-tyrosine. *Colloids Surf. B Biointerfaces* 101, 183–188. <https://doi.org/10.1016/j.colsurfb.2012.06.007>
 29. Deng, S., Berry, V., 2016. Wrinkled, rippled and crumpled graphene: an overview of formation mechanism, electronic properties, and applications. *Mater. Today* 19, 197–212. <https://doi.org/10.1016/j.mattod.2015.10.002>
 30. Dong, L., Yang, J., Chhowalla, M., Ping Loh, K., 2017. Synthesis and reduction of large sized graphene oxide sheets. *Chem. Soc. Rev.* 46, 7306–7316. <https://doi.org/10.1039/C7CS00485K>
 31. Emiru, T.F., Ayele, D.W., 2017. Controlled synthesis, characterization and reduction of graphene oxide: A convenient method for large scale production. *Egypt. J. Basic Appl. Sci.* 4, 74–79. <https://doi.org/10.1016/j.ejbas.2016.11.002>
 32. Fadil, Y., Dinh, L.N.M., Yap, M.O.Y., Kuchel, R.P., Yao, Y., Omura, T., Aregueta-Robles, U.A., Song, N., Huang, S., Jasinski, F., Thickett, S.C., Minami, H., Agarwal, V., Zetterlund, P.B., 2019. Ambient-Temperature Waterborne Polymer/rGO Nanocomposite Films: Effect of rGO Distribution on Electrical Conductivity. *ACS Appl. Mater. Interfaces* 11, 48450–48458. <https://doi.org/10.1021/acsami.9b19183>
 33. Fan, M., Hu, J., Cao, R., Xiong, K., Wei, X., 2017. Modeling and prediction of copper removal from aqueous solutions by nZVI/rGO magnetic nanocomposites using ANN-GA and ANN-PSO. *Sci. Rep.* 7, 18040. <https://doi.org/10.1038/s41598-017-18223-y>
 34. Farhan, S.N., Ismael, M.H., Mahmood, W.A., Khadom, A.A., Karim, A.M.A., 2021. Biosorption of Copper and Lead Ions Using Chara Algae. *Pak. J. Eng. Appl. Sci.* 1–6.
 35. Gabris, M.A., Jume, B.H., Rezaali, M., Shahabuddin, S., Nodeh, H.R., Saidur, R., 2018. Novel magnetic graphene oxide functionalized cyanopropyl nanocomposite as an adsorbent for the removal of Pb(II) ions from aqueous media: equilibrium and kinetic studies. *Environ. Sci. Pollut. Res.* 25, 27122–27132. <https://doi.org/10.1007/s11356-018-2749-9>
 36. Gan, L., Li, B., Chen, Y., Yu, B., Chen, Z., 2019. Green synthesis of reduced graphene oxide using bagasse and its application in dye removal: A waste-to-resource supply chain. *Chemosphere* 219, 148–154. <https://doi.org/10.1016/j.chemosphere.2018.11.181>
 37. Gao, J., Sun, S.-P., Zhu, W.-P., Chung, T.-S., 2014. Chelating polymer modified P84 nanofiltration (NF) hollow fiber membranes for high efficient heavy metal removal. *Water Res.* 63, 252–261. <https://doi.org/10.1016/j.watres.2014.06.006>
 38. GB 25467, 2010. Emission standard of pollutants for copper, nickel, cobalt industry (No. GB 25467 —2010). Department of science and technology standards, Ministry of environmental protection, China.
 39. Guo, H., Bi, C., Zeng, C., Ma, W., Yan, L., Li, K., Wei, K., 2018. Camellia oleifera seed shell carbon as an efficient renewable bio-adsorbent for the adsorption removal of hexavalent chromium and methylene blue from aqueous solution. *J. Mol. Liq.* 249, 629–636. <https://doi.org/10.1016/j.molliq.2017.11.096>
 40. Guo, T., Bulin, C., Li, B., Zhao, Z., Yu, H., Sun, H., Ge, X., Xing, R., Zhang, B., 2018. Efficient removal of aqueous Pb(II) using partially reduced graphene oxide-Fe₃O₄. *Adsorpt. Sci. Technol.* 36, 1031–1048. <https://doi.org/10.1177/0263617417744402>

41. Hao, J., Han, M.-J., Meng, X., 2009. Preparation and evaluation of thiol-functionalized activated alumina for arsenite removal from water. *J. Hazard. Mater.* 167, 1215–1221. <https://doi.org/10.1016/j.jhazmat.2009.01.124>
42. Hou, D., Liu, Q., Cheng, H., Li, K., Wang, D., Zhang, H., 2016. Chrysanthemum extract assisted green reduction of graphene oxide. *Mater. Chem. Phys.* 183, 76–82. <https://doi.org/10.1016/j.matchemphys.2016.08.004>
43. Hu, X., Yu, Y., Hou, W., Zhou, J., Song, L., 2013. Effects of particle size and pH value on the hydrophilicity of graphene oxide. *Appl. Surf. Sci.* 273, 118–121. <https://doi.org/10.1016/j.apsusc.2013.01.201>
44. Huang, L., Weng, X., Chen, Z., Megharaj, M., Naidu, R., 2014. Synthesis of iron-based nanoparticles using oolong tea extract for the degradation of malachite green. *Spectrochim. Acta. A. Mol. Biomol. Spectrosc.* 117, 801–804. <https://doi.org/10.1016/j.saa.2013.09.054>
45. Huiping, S., Xingang, L., Huaigang, C., Fangqin, C., 2013. Theoretical and experimental study of Au(III)-containing wastewater treatment using magnetotactic bacteria. *Desalination Water Treat.* 51, 3864–3870. <https://doi.org/10.1080/19443994.2013.781737>
46. Hylling, O., Nikbakht Fini, M., Ellegaard-Jensen, L., Muff, J., Madsen, H.T., Aamand, J., Hansen, L.H., 2019. A novel hybrid concept for implementation in drinking water treatment targets micropollutant removal by combining membrane filtration with biodegradation. *Sci. Total Environ.* 694, 133710. <https://doi.org/10.1016/j.scitotenv.2019.133710>
47. Ioannou-Ttofa, L., Raj, S., Prakash, H., Fatta-Kassinos, D., 2019. Solar photo-Fenton oxidation for the removal of ampicillin, total cultivable and resistant *E. coli* and ecotoxicity from secondary-treated wastewater effluents. *Chem. Eng. J.* 355, 91–102. <https://doi.org/10.1016/j.cej.2018.08.057>
48. Javed, I., Mateen, F., Rafique, U., Tabassum, N., Balkhair, K., Ashraf, M., 2015. Synthesis of zeolite from marble powder waste: a greener approach and its application for the removal of inorganic metals from wastewater. *Desalination Water Treat.* 57, 1–10. <https://doi.org/10.1080/19443994.2015.1033763>
49. Jiang, H., 2015. A preliminary study on the extraction and purification of tea saponins from oil tea seed husks and their properties (Master degree thesis). Shanghai Normal University, China.
50. Kainthola, J., Kalamdhad, A.S., Goud, V.V., 2019. Optimization of methane production during anaerobic co-digestion of rice straw and *hydrilla verticillata* using response surface methodology. *Fuel* 235, 92–99. <https://doi.org/10.1016/j.fuel.2018.07.094>
51. Kayalvizhi, K., Alhaji, N.M.I., Saravanakkumar, D., Mohamed, S.B., Kaviyarasu, K., Ayeshamariam, A., Al-Mohaimed, A.M., AbdelGawwad, M.R., Elshikh, M.S., 2022. Adsorption of copper and nickel by using sawdust chitosan nanocomposite beads – A kinetic and thermodynamic study. *Environ. Res.* 203, 111814. <https://doi.org/10.1016/j.envres.2021.111814>
52. Kayranli, B., Gok, O., Yilmaz, T., Gok, G., Celebi, H., Seckin, I.Y., Kalat, D., 2021. Zinc Removal Mechanisms with Recycled Lignocellulose: from Fruit Residual to Biosorbent then Soil Conditioner. *Water. Air. Soil Pollut.* 232, 311. <https://doi.org/10.1007/s11270-021-05260-7>
53. Khan, Mujeeb, Al-Marri, A.H., Khan, Merajuddin, Mohri, N., Adil, S.F., Al-Warthan, A., Siddiqui, M.R.H., Alkathlan, H.Z., Berger, R., Tremel, W., Tahir, M.N., 2014. *Pulicaria*

- glutinosa plant extract: a green and eco-friendly reducing agent for the preparation of highly reduced graphene oxide. *RSC Adv.* 4, 24119–24125. <https://doi.org/10.1039/C4RA01296H>
54. Khobragade, M.U., Nayak, A.K., Pal, A., 2016. Application of response surface methodology to evaluate the removal efficiency of Mn(II), Ni(II), and Cu(II) by surfactant-modified alumina. *Clean Technol. Environ. Policy* 18, 1003–1020. <https://doi.org/10.1007/s10098-016-1116-0>
 55. Kichukova, D., Spassova, I., Kostadinova, A., Staneva, A., Kovacheva, D., 2022. Facile Synthesized Cu–RGO and Ag–RGO Nanocomposites with Potential Biomedical Applications. *Nanomaterials* 12, 2096. <https://doi.org/10.3390/nano12122096>
 56. Kumar, S., Jain, S., 2013. History, Introduction, and Kinetics of Ion Exchange Materials. *J. Chem.* 2013, e957647. <https://doi.org/10.1155/2013/957647>
 57. Lata, S., Singh, P.K., Samadder, S.R., 2015. Regeneration of adsorbents and recovery of heavy metals: a review. *Int. J. Environ. Sci. Technol.* 12, 1461–1478. <https://doi.org/10.1007/s13762-014-0714-9>
 58. Li, B., Jin, X., Lin, J., Chen, Z., 2018. Green reduction of graphene oxide by sugarcane bagasse extract and its application for the removal of cadmium in aqueous solution. *J. Clean. Prod.* 189, 128–134. <https://doi.org/10.1016/j.jclepro.2018.04.018>
 59. Li, C., Zhuang, Z., Jin, X., Chen, Z., 2017. A facile and green preparation of reduced graphene oxide using *Eucalyptus* leaf extract. *Appl. Surf. Sci.* 422, 469–474. <https://doi.org/10.1016/j.apsusc.2017.06.032>
 60. Li, H., Huang, Y., Liu, J., Duan, H., 2021. Hydrothermally synthesized titanate nanomaterials for the removal of heavy metals and radionuclides from water: A review. *Chemosphere* 282, 131046. <https://doi.org/10.1016/j.chemosphere.2021.131046>
 61. Li, T., Liu, X., Li, L., Wang, Y., Ma, P., Chen, M., Dong, W., 2019. Polydopamine-functionalized graphene oxide compounded with polyvinyl alcohol/chitosan hydrogels on the recyclable adsorption of Cu(II), Pb(II) and Cd(II) from aqueous solution. *J. Polym. Res.* 26, 281. <https://doi.org/10.1007/s10965-019-1971-6>
 62. Li, Z., Wang, L., Meng, J., Liu, X., Xu, J., Wang, F., Brookes, P., 2018. Zeolite-supported nanoscale zero-valent iron: New findings on simultaneous adsorption of Cd(II), Pb(II), and As(III) in aqueous solution and soil. *J. Hazard. Mater.* 344, 1–11. <https://doi.org/10.1016/j.jhazmat.2017.09.036>
 63. Lin, T.-Y., Chen, D.-H., 2014. One-step green synthesis of arginine-capped iron oxide/reduced graphene oxide nanocomposite and its use for acid dye removal. *RSC Adv.* 4, 29357–29364. <https://doi.org/10.1039/C4RA03505D>
 64. Lin, Z., Weng, X., Owens, G., Chen, Z., 2020. Simultaneous removal of Pb(II) and rifampicin from wastewater by iron nanoparticles synthesized by a tea extract. *J. Clean. Prod.* 242, 118476. <https://doi.org/10.1016/j.jclepro.2019.118476>
 65. Liu, L., Li, C., Bao, C., Jia, Q., Xiao, P., Liu, X., Zhang, Q., 2012. Preparation and characterization of chitosan/graphene oxide composites for the adsorption of Au(III) and Pd(II). *Talanta* 93, 350–357. <https://doi.org/10.1016/j.talanta.2012.02.051>
 66. Liu, Y., Li, X., Wang, Y., Zhou, J., He, W., 2019a. Preparation and Characterization of *Camellia oleifera* Nut Shell-based Bioadsorbent and its Application for Heavy Metals Removal. *BioResources* 14, 234–250.
 67. Liu, Y., Li, X., Wang, Y., Zhou, J., He, W., 2019b. Preparation and Characterization of

- Camellia oleifera Nut Shell-based Bioadsorbent and its Application for Heavy Metals Removal. *BioResources* 14, 234–250.
68. Lu, X., Wang, F., Li, X., Shih, K., Zeng, E.Y., 2016. Adsorption and Thermal Stabilization of Pb^{2+} and Cu^{2+} by Zeolite. *Ind. Eng. Chem. Res.* 55, 8767–8773. <https://doi.org/10.1021/acs.iecr.6b00896>
 69. Luo, Z., Yao, B., Yang, X., Wang, L., Xu, Z., Yan, X., Tian, L., Zhou, H., Zhou, Y., 2022. Novel insights into the adsorption of organic contaminants by biochar: A review. *Chemosphere* 287, 132113. <https://doi.org/10.1016/j.chemosphere.2021.132113>
 70. Ma, W.S., Zhou, J.W., Lin, X.D., 2011. X-Ray Photoelectron Spectroscopy Study on Reduction of Graphene Oxide with Hydrazine Hydrate. *Adv. Mater. Res.* 287–290, 539–543. <https://doi.org/10.4028/www.scientific.net/AMR.287-290.539>
 71. Mahmudzadeh, M., Yari, H., Ramezanzadeh, B., Mahdavian, M., 2019. Highly potent radical scavenging-anti-oxidant activity of biologically reduced graphene oxide using *Nettle* extract as a green bio-genic amines-based reductants source instead of hazardous hydrazine hydrate. *J. Hazard. Mater.* 371, 609–624. <https://doi.org/10.1016/j.jhazmat.2019.03.046>
 72. Malhotra, N., Ger, T.-R., Uapipatanakul, B., Huang, J.-C., Chen, K.H.-C., Hsiao, C.-D., 2020. Review of Copper and Copper Nanoparticle Toxicity in Fish. *Nanomaterials* 10, 1126. <https://doi.org/10.3390/nano10061126>
 73. Mata, Y.N., Blázquez, M.L., Ballester, A., González, F., Muñoz, J.A., 2009. Sugar-beet pulp pectin gels as biosorbent for heavy metals: Preparation and determination of biosorption and desorption characteristics. *Chem. Eng. J.* 150, 289–301. <https://doi.org/10.1016/j.cej.2009.01.001>
 74. Meringer, A., Liffourrena, A.S., Heredia, R.M., Lucchesi, G.I., Boeris, P.S., 2021. Removal of copper and/or zinc ions from synthetic solutions by immobilized, non-viable bacterial biomass: Batch and fixed-bed column lab-scale study. *J. Biotechnol.* 328, 87–94. <https://doi.org/10.1016/j.jbiotec.2021.01.011>
 75. Mokone, T.P., van Hille, R.P., Lewis, A.E., 2010. Effect of solution chemistry on particle characteristics during metal sulfide precipitation. *J. Colloid Interface Sci.* 351, 10–18. <https://doi.org/10.1016/j.jcis.2010.06.027>
 76. Naushad, M., 2014. Surfactant assisted nano-composite cation exchanger: Development, characterization and applications for the removal of toxic Pb^{2+} from aqueous medium. *Chem. Eng. J.* 235, 100–108. <https://doi.org/10.1016/j.cej.2013.09.013>
 77. Nayak, A., Bhushan, B., 2021. Hydroxyapatite as an advanced adsorbent for removal of heavy metal ions from water: Focus on its applications and limitations. *Mater. Today Proc.*, International Conference on Technological Advancements in Materials Science and Manufacturing 46, 11029–11034. <https://doi.org/10.1016/j.matpr.2021.02.149>
 78. Nie, Z., Huang, Y., Ma, B., Qiu, X., Zhang, N., Xie, X., Wu, Z., 2019. Nitrogen-doped Carbon with Modulated Surface Chemistry and Porous Structure by a Stepwise Biomass Activation Process towards Enhanced Electrochemical Lithium-Ion Storage. *Sci. Rep.* 9, 15032. <https://doi.org/10.1038/s41598-019-50330-w>
 79. Novoselov, K.S., Geim, A.K., Morozov, S.V., Jiang, D., Zhang, Y., Dubonos, S.V., Grigorieva, I.V., Firsov, A.A., 2004. Electric Field Effect in Atomically Thin Carbon Films. *Science* 306, 666–669. <https://doi.org/10.1126/science.1102896>
 80. Oh, W.-D., Lee, M.G.-H., Chanaka Udayanga, W.D., Veksha, A., Bao, Y., Giannis, A., Lim,

- J.-W., Lisak, G., 2019. Insights into the single and binary adsorption of copper(II) and nickel(II) on hexagonal boron nitride: Performance and mechanistic studies. *J. Environ. Chem. Eng.* 7, 102872. <https://doi.org/10.1016/j.jece.2018.102872>
81. Ong, S.-Q., Lee, B.-B., Tan, G.-P., Maniam, S., 2017. Capacity of black soldier fly and house fly larvae in treating the wasted rice in Malaysia. *Malays. J. Sustain. Agric.* 1, 08–10. <https://doi.org/10.26480/mjsa.01.2017.08.10>
 82. Peng, Q., Guo, J., Zhang, Q., Xiang, J., Liu, B., Zhou, A., Liu, R., Tian, Y., 2014. Unique Lead Adsorption Behavior of Activated Hydroxyl Group in Two-Dimensional Titanium Carbide. *J. Am. Chem. Soc.* 136, 4113–4116. <https://doi.org/10.1021/ja500506k>
 83. Perez Mora, B., Bellú, S., Mangiameli, M.F., Frascaroli, M.I., González, J.C., 2019. Response surface methodology and optimization of arsenic continuous sorption process from contaminated water using chitosan. *J. Water Process Eng.* 32, 100913. <https://doi.org/10.1016/j.jwpe.2019.100913>
 84. Qiu, L., Wan, W., Tong, Z., Zhang, R., Li, L., Zhou, Y., 2018. Controllable and green synthesis of robust graphene aerogels with tunable surface properties for oil and dye adsorption. *New J. Chem.* 42, 1003–1009. <https://doi.org/10.1039/C7NJ03329J>
 85. Riveros, P.A., 2010. The removal of antimony from copper electrolytes using amino-phosphonic resins: Improving the elution of pentavalent antimony. *Hydrometallurgy* 105, 110–114. <https://doi.org/10.1016/j.hydromet.2010.08.008>
 86. Sadhukhan, S., Ghosh, T.K., Rana, D., Roy, I., Bhattacharyya, A., Sarkar, G., Chakraborty, M., Chattopadhyay, D., 2016. Studies on synthesis of reduced graphene oxide (RGO) via green route and its electrical property. *Mater. Res. Bull.* 79, 41–51. <https://doi.org/10.1016/j.materresbull.2016.02.039>
 87. Sahari, M.A., Ataii, D., Hamedi, M., 2004. Characteristics of tea seed oil in comparison with sunflower and olive oils and its effect as a natural antioxidant. *J. Am. Oil Chem. Soc.* 81, 585–588. <https://doi.org/10.1007/s11746-006-0945-0>
 88. Saleem, H., Haneef, M., Abbasi, H.Y., 2018. Synthesis route of reduced graphene oxide via thermal reduction of chemically exfoliated graphene oxide. *Mater. Chem. Phys.* 204, 1–7. <https://doi.org/10.1016/j.matchemphys.2017.10.020>
 89. Schouwenaars, R., Montoya-Bautista, C.V., Isaacs-Páez, E.D., Solís-López, M., Ramírez-Zamora, R.M., 2017. Removal of arsenic III and V from laboratory solutions and contaminated groundwater by metallurgical slag through anion-induced precipitation. *Environ. Sci. Pollut. Res.* 24, 25034–25046. <https://doi.org/10.1007/s11356-017-0120-1>
 90. Severino, F., Brito, J.L., Laine, J., Fierro, J.L.G., Agudo, A.L., 1998. Nature of Copper Active Sites in the Carbon Monoxide Oxidation on CuAl_2O_4 and CuCr_2O_4 Spinel Type Catalysts. *J. Catal.* 177, 82–95. <https://doi.org/10.1006/jcat.1998.2094>
 91. Sharma, G., Kumar, A., Naushad, Mu., García-Peñas, A., Al-Muhtaseb, A.H., Ghfar, A.A., Sharma, V., Ahamad, T., Stadler, F.J., 2018. Fabrication and characterization of Gum arabic-*c*-poly(acrylamide) nanohydrogel for effective adsorption of crystal violet dye. *Carbohydr. Polym.* 202, 444–453. <https://doi.org/10.1016/j.carbpol.2018.09.004>
 92. Shen, Y., Chen, B., 2015. Sulfonated Graphene Nanosheets as a Superb Adsorbent for Various Environmental Pollutants in Water. *Environ. Sci. Technol.* 49, 7364–7372. <https://doi.org/10.1021/acs.est.5b01057>
 93. Shen, Y., Fang, Q., Chen, B., 2015. Environmental Applications of Three-Dimensional

- Graphene-Based Macrostructures: Adsorption, Transformation, and Detection. *Environ. Sci. Technol.* 49, 67–84. <https://doi.org/10.1021/es504421y>
94. Song, X., Li, L., Geng, Z., Zhou, L., Ji, L., 2017. Effective and selective adsorption of As(III) via imprinted magnetic Fe₃O₄/HTCC composite nanoparticles. *J. Environ. Chem. Eng.* 5, 16–25. <https://doi.org/10.1016/j.jece.2016.11.016>
 95. Sprynskyy, M., Kowalkowski, T., Tutu, H., Cukrowska, E.M., Buszewski, B., 2015. Ionic liquid modified diatomite as a new effective adsorbent for uranium ions removal from aqueous solution. *Colloids Surf. Physicochem. Eng. Asp.* 465, 159–167. <https://doi.org/10.1016/j.colsurfa.2014.10.042>
 96. Sramala, I., Pinket, W., Pongwan, P., Jarussophon, S., Kasemwong, K., 2016. Development of an *in Vitro* System to Simulate the Adsorption of Self-Emulsifying Tea (*Camellia oleifera*) Seed Oil. *Molecules* 21, 479. <https://doi.org/10.3390/molecules21050479>
 97. Sun, H., Sun, L., Zhao, Y., Yang, S., Zhang, L., Dong, H., Yuan, H., Ling, Z., Zhao, J., Song, Y., 2021. A combined hydrate-based method for removing heavy metals from simulated wastewater with high concentrations. *J. Environ. Chem. Eng.* 9, 106633. <https://doi.org/10.1016/j.jece.2021.106633>
 98. Thangavel, S., Venugopal, G., 2014. Understanding the adsorption property of graphene-oxide with different degrees of oxidation levels. *Powder Technol.* 257, 141–148. <https://doi.org/10.1016/j.powtec.2014.02.046>
 99. Tsukamoto, S., Kanegae, T., Nagoya, T., Shimamura, M., Kato, T., Watanabe, S., Kawaguchi, M., 1993. Effects of Seed Saponins of *Thea Sinensis* L. (Ryokucha Saponin) on Alcohol Absorption and Metabolism. *Alcohol Alcohol* 28, 687–692. <https://doi.org/10.1093/oxfordjournals.alcalc.a045455>
 100. US EPA, O., 2015. Secondary Drinking Water Standards: Guidance for Nuisance Chemicals [WWW Document]. URL <https://www.epa.gov/sdwa/secondary-drinking-water-standards-guidance-nuisance-chemicals> (accessed 9.5.22).
 101. V. Chaban, V., V. Prezhdo, O., 2017. Microwave reduction of graphene oxide rationalized by reactive molecular dynamics. *Nanoscale* 9, 4024–4033. <https://doi.org/10.1039/C7NR00341B>
 102. Velusamy, S., Roy, A., Sundaram, S., Mallick, T., 2021. A Review on Heavy Metal Ions and Containing Dyes Removal Through Graphene Oxide-Based Adsorption Strategies for Textile Wastewater Treatment. *Chem. Rec. N. Y. N* 21. <https://doi.org/10.1002/tcr.202000153>
 103. Wang, T., Lin, J., Chen, Z., Megharaj, M., Naidu, R., 2014. Green synthesized iron nanoparticles by green tea and eucalyptus leaves extracts used for removal of nitrate in aqueous solution. *J. Clean. Prod.* 83, 413–419. <https://doi.org/10.1016/j.jclepro.2014.07.006>
 104. Wei, Z., Wang, D., Kim, S., Kim, S.-Y., Hu, Y., Yakes, M.K., Laracuate, A.R., Dai, Z., Marder, S.R., Berger, C., King, W.P., de Heer, W.A., Sheehan, P.E., Riedo, E., 2010. Nanoscale Tunable Reduction of Graphene Oxide for Graphene Electronics. *Science* 328, 1373–1376. <https://doi.org/10.1126/science.1188119>
 105. Weng, X., Wu, J., Ma, L., Owens, G., Chen, Z., 2019. Impact of synthesis conditions on Pb(II) removal efficiency from aqueous solution by green tea extract reduced graphene oxide. *Chem. Eng. J.* 359, 976–981. <https://doi.org/10.1016/j.cej.2018.11.089>
 106. WHO, 2017. Guidelines for drinking-water quality: Fourth edition incorporating the first and second addenda. World Health Organization, Geneva.
 107. Xie, Y., Ge, S., Jiang, S., Liu, Z., Chen, L., Wang, L., Chen, J., Qin, L., Peng, W., 2018. Study

- on biomolecules in extractives of *Camellia oleifera* fruit shell by GC–MS. Saudi J. Biol. Sci. 25, 234–236. <https://doi.org/10.1016/j.sjbs.2017.08.006>
108. Xie, Y., Yuan, X., Wu, Z., Zeng, G., Jiang, L., Peng, X., Li, H., 2019. Adsorption behavior and mechanism of Mg/Fe layered double hydroxide with Fe₃O₄-carbon spheres on the removal of Pb(II) and Cu(II). J. Colloid Interface Sci. 536, 440–455. <https://doi.org/10.1016/j.jcis.2018.10.066>
 109. Yan, W., Herzing, A.A., Kiely, C.J., Zhang, W., 2010. Nanoscale zero-valent iron (nZVI): Aspects of the core-shell structure and reactions with inorganic species in water. J. Contam. Hydrol., Manufactured Nanomaterials in Subsurface Systems 118, 96–104. <https://doi.org/10.1016/j.jconhyd.2010.09.003>
 110. Yang, X., Chen, C., Li, J., Zhao, G., Ren, X., Wang, X., 2012. Graphene oxide- iron oxide and reduced graphene oxide - iron oxide hybrid materials for the removal of organic and inorganic pollutants. RSC Adv. 2, 8821–8826. <https://doi.org/10.1039/C2RA20885G>
 111. Ye, X., Shang, S., Zhao, Y., Cui, S., Zhong, Y., Huang, L., 2021. Ultra-efficient adsorption of copper ions in chitosan–montmorillonite composite aerogel at wastewater treatment. Cellulose 28, 7201–7212. <https://doi.org/10.1007/s10570-021-03976-7>
 112. Ye, Y., Guo, Y., Luo, Y.-T., Wang, Y.-F., 2012. Isolation and free radical scavenging activities of a novel biflavonoid from the shells of *Camellia oleifera* Abel. Fitoterapia, Prof. Atta-ur-Rahman FRS (70th B'Day) 83, 1585–1589. <https://doi.org/10.1016/j.fitote.2012.09.006>
 113. Yi, Z., Liu, J., Zeng, R., Liu, X., Long, J., Huang, B., 2020. Removal of uranium (VI) from aqueous solution by *Camellia oleifera* shell-based activated carbon: adsorption equilibrium, kinetics, and thermodynamics. Water Sci. Technol. 82, 2592–2602. <https://doi.org/10.2166/wst.2020.504>
 114. Zare Pirhaji, J., Moeinpour, F., Mirhoseini Dehabadi, A., Yasini Ardakani, S.A., 2020. Synthesis and characterization of halloysite/graphene quantum dots magnetic nanocomposite as a new adsorbent for Pb(II) removal from water. J. Mol. Liq. 300, 112345. <https://doi.org/10.1016/j.molliq.2019.112345>
 115. Zhang, B., Han, X., Gu, P., Fang, S., Bai, J., 2017. Response surface methodology approach for optimization of ciprofloxacin adsorption using activated carbon derived from the residue of desiccated rice husk. J. Mol. Liq. 238, 316–325. <https://doi.org/10.1016/j.molliq.2017.04.022>
 116. Zhang, D., Stack, L., Zhang, R., Yu, J., Xie, B., Ruter, J., 2006. Tea oil Camellia - Eastern “Olive” for the World. Acta Hort. 769. <https://doi.org/10.17660/ActaHortic.2008.769.3>
 117. Zhang, Jiali, Yang, H., Shen, G., Cheng, P., Zhang, Jingyan, Guo, S., 2010. Reduction of graphene oxide via L-ascorbic acid. Chem. Commun. 46, 1112–1114. <https://doi.org/10.1039/B917705A>
 118. Zhang, K., Li, H., Xu, X., Yu, H., 2018. Synthesis of reduced graphene oxide/NiO nanocomposites for the removal of Cr(VI) from aqueous water by adsorption. Microporous Mesoporous Mater. 255, 7–14. <https://doi.org/10.1016/j.micromeso.2017.07.037>
 119. Zhang, Y., Chen, Q., Luo, X., Dai, T., Lu, B., Shen, J., 2011. Mutagenicity and Safety Evaluation of the Water Extract of *Camellia oleifera* Abel. J. Food Sci. 76, T84–T89. <https://doi.org/10.1111/j.1750-3841.2011.02101.x>
 120. Zhang, Y., Chi, H., Zhang, W., Sun, Y., Liang, Q., Gu, Y., Jing, R., 2014. Highly Efficient Adsorption of Copper Ions by a PVP-Reduced Graphene Oxide Based On a New Adsorptions

- Mechanism. *Nano-Micro Lett.* 6, 80–87. <https://doi.org/10.1007/BF03353772>
121. Zhang, Y., Duan, X., 2020. Chemical precipitation of heavy metals from wastewater by using the synthetical magnesium hydroxy carbonate. *Water Sci. Technol.* 81, 1130–1136. <https://doi.org/10.2166/wst.2020.208>
 122. Zhao, Y., Su, R., Zhang, W., Yao, G.-L., Chen, J., 2020. Antibacterial activity of tea saponin from *Camellia oleifera* shell by novel extraction method. *Ind. Crops Prod.* 153, 112604. <https://doi.org/10.1016/j.indcrop.2020.112604>
 123. Zhou, M., Wang, Y., Zhai, Y., Zhai, J., Ren, W., Wang, F., Dong, S., 2009. Controlled Synthesis of Large-Area and Patterned Electrochemically Reduced Graphene Oxide Films. *Chem. – Eur. J.* 15, 6116–6120. <https://doi.org/10.1002/chem.200900596>
 124. Zhu, J., Zhu, Y., Jiang, F., Xu, Y., Ouyang, J., Yu, S., 2013. An integrated process to produce ethanol, vanillin, and xylooligosaccharides from *Camellia oleifera* shell. *Carbohydr. Res.* 382, 52–57. <https://doi.org/10.1016/j.carres.2013.10.007>